

Understanding the sign problem from an exact Path Integral Monte Carlo model of interacting harmonic fermions

Siu A. Chin*

Department of Physics and Astronomy,

Texas A&M University, College Station, TX 77843, USA

Abstract

This work shows that the recently discovered operator contraction identity for solving the discrete Path Integral of the harmonic oscillator can be applied equally to fermions in any dimension. This then yields an exactly solvable model for studying the sign problem where the Path Integral Monte Carlo energy at any time step for any number of fermions is known analytically, or can be computed numerically. It is found that repulsive/attractive pairwise interaction shifts the sign problem to larger/smaller imaginary time, but does not make it more severe than the non-interacting case. More surprisingly, for closed-shell number of fermions, the sign problem goes away at large imaginary time. Fourth-order and newly found variable-bead algorithms are used to compute ground state energies of quantum dots with up to 110 electrons and compared to results obtained by modern neural networks.

I. INTRODUCTION

Recent advances in Path Integral Monte Carlo (PIMC) continue to be the use of parameterized fourth-order propagators to optimize PIMC's convergence at the fewest number of beads/time-slices for both bosons¹⁻⁸ and fermions⁹⁻¹¹. While this increase in efficiency is useful for both, it is of crucial importance for fermions because its sign problem worsens with increasing number of beads. However, because there is no simple model for understanding PIMC for fermions at each time step, one's knowledge of the sign problem remains scant. For example, it is well known since Takahashi and Imada's calculation¹² 40 years ago that PIMC has no sign problem in one dimension. Yet, an explicit proof¹³ of this has only appeared recently. The technique used in that proof can now be generalized to explain why there is no sign problem for closed-shell particle states at large imaginary time. (See Sect.VII below.)

In a previous work¹⁴, because of an operator contraction identity, this author discovered the *universal* PIMC discrete propagator for the harmonic oscillator, which has the same functional form for all initial short-time propagators. Each short-time propagator only modifies the argument of the universal coefficient functions. This then makes it possible to obtain physical observables in closed forms for all short-time propagators at once. In particular, one can compute the thermodynamic and Hamiltonian energies analytically at each discrete imaginary time step for any short-time propagator¹⁵.

This work now shows that this contraction identity remains valid for the anti-symmetric determinant fermion propagator at all dimensions and for any number of fermions. Therefore, one has a completely solvable PIMC model of harmonic fermions with analytical thermodynamic and Hamiltonian energies. Moreover, the model remains solvable if the pairwise interaction is also harmonic. Therefore, the sign problem can be examined in detail, with and without interactions.

In Section II, we review the contraction identity for the harmonic oscillator in one dimension, then generalize it to any number of fermions in any dimension. By use of this contraction, Sect.III summarizes the universal discrete PIMC propagator for harmonic fermions. Sect.IV derives the analytical form of the discrete partition function at each time-step for all short-time propagators. Sect.V gives the analytical thermodynamic and Hamiltonian fermion energies at each discrete time-step verified by direct PIMC simulation. Sect.VI

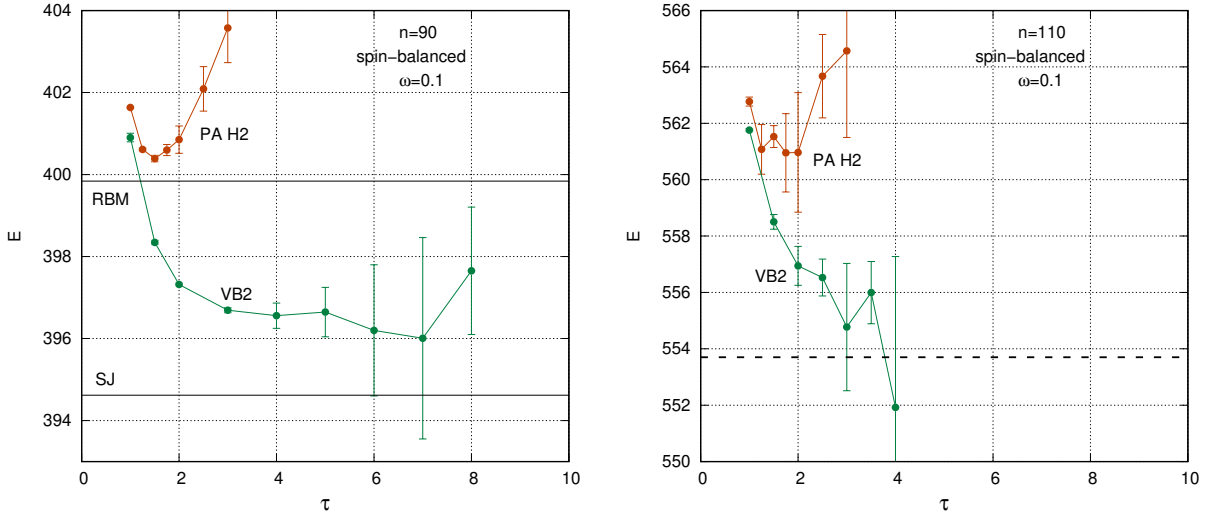


FIG. 1: (color online) **Left:** The Hamiltonian energy of a 90-electron unpolarized quantum dot as a function of imaginary time τ . Algorithm VB2's energy of 396.69(6) at $\tau = 3$, is only 0.5% above Ref.16's SJ neural network energy of 394.621(4). **Right:** The Hamiltonian energy for a 110-electron unpolarized quantum dot. Algorithm VB2's energy at $\tau = 2.5$ is 556.5(6). See Sect.X for details.

discusses the PIMC fermion sign problem and the empirical finding that there is no sign problem for closed-shell particle states at large imaginary time. Sect.VII explains the surprising connection between the absence of the sign problem in one dimension and in closed-shell particle states. Sect.VIII shows how pairwise interactions, both harmonic and Coulombic, modify the sign problem from the non-interacting case. For spin-balanced quantum dots, Sect.IX shows that fourth-order algorithms give excellent ground state energies for less than 30 electrons, provided that the Coulomb interaction is sufficiently repulsive. Larger quantum dots necessitate the use of a new class of Variable-Bead algorithms in Sect.X. The ensuing energy for a 90-electron quantum dot is compared to modern neural network¹⁶ results in Fig.1. Some concluding remarks are given in Sect.XI.

II. FREE FERMION PROPAGATOR CONTRACTIONS

For the dimensionless harmonic oscillator Hamiltonian in 1D given by

$$\hat{H} = -\frac{1}{2} \frac{d^2}{dx^2} + \frac{1}{2} x^2 \equiv \hat{T} + \hat{V}, \quad (2.1)$$

as shown in Ref.14, the Gaussian integral needed to compute the discrete path integral is given by

$$\langle x' | e^{-a\hat{T}} e^{-b\hat{V}} e^{-c\hat{T}} | x^* \rangle = \frac{1}{\sqrt{2\pi a}} \frac{1}{\sqrt{2\pi c}} \int_{-\infty}^{\infty} dx e^{-\frac{1}{2a}(x'-x)^2 - b\frac{1}{2}x^2 - \frac{1}{2c}(x-x^*)^2} \quad (2.2)$$

$$= \frac{1}{\sqrt{2\pi\kappa}} e^{-\nu\frac{1}{2}x'^2} e^{-\frac{1}{2\kappa}(x'-x^*)^2} e^{-\mu\frac{1}{2}x^{*2}} \quad (2.3)$$

$$= \langle x' | e^{-\nu\hat{V}} e^{-\kappa\hat{T}} e^{-\mu\hat{V}} | x^* \rangle \quad (2.4)$$

with

$$\kappa = a + abc + c, \quad \nu = \frac{bc}{\kappa}, \quad \mu = \frac{ba}{\kappa}. \quad (2.5)$$

This means that one actually has an operator identity

$$e^{-a\hat{T}} e^{-b\hat{V}} e^{-c\hat{T}} = e^{-\nu\hat{V}} e^{-\kappa\hat{T}} e^{-\mu\hat{V}}, \quad (2.6)$$

which contracts two free particle propagators $e^{-a\hat{T}}$ and $e^{-c\hat{T}}$ into one $e^{-\kappa\hat{T}}$. Therefore any discrete path integral of the harmonic oscillator can be contracted down to a single free propagator form and be evaluated analytically as

$$\langle x' | e^{-A\hat{V}} e^{-B\hat{T}} e^{-C\hat{V}} | x \rangle = e^{-A\frac{1}{2}x'^2} \frac{1}{\sqrt{2\pi B}} e^{-\frac{1}{2B}(x'-x)^2} e^{-C\frac{1}{2}x^2}. \quad (2.7)$$

Consider the case of n -particles in D -dimension with configuration vector $\mathbf{x} = (\mathbf{r}_1, \mathbf{r}_2, \dots, \mathbf{r}_n)$ where each particle position vector is $\mathbf{r} = (x_1, x_2, \dots, x_D)$. Since the harmonic oscillator is separable in each coordinate, the contraction (2.6) now holds for

$$\hat{T} = -\frac{1}{2}\nabla_{\mathbf{x}}^2 = -\frac{1}{2}\sum_{i=1}^n \nabla_i^2 \quad \text{and} \quad \hat{V} = \frac{1}{2}\mathbf{x}^2 = \frac{1}{2}\sum_{i=1}^n \mathbf{r}_i^2 \quad (2.8)$$

where the n -particle free propagator is given by

$$\begin{aligned} g_0(\mathbf{x}', \mathbf{x}, \epsilon) &= \langle \mathbf{x}' | e^{-\epsilon\hat{T}} | \mathbf{x} \rangle \\ &= \frac{1}{(2\pi\epsilon)^{nD/2}} \exp\left[-\frac{1}{2\epsilon}(\mathbf{x}' - \mathbf{x})^2\right] \\ &= \prod_{i=1}^n \frac{1}{(2\pi\epsilon)^{D/2}} \exp\left[-\frac{1}{2\epsilon}(\mathbf{r}'_i - \mathbf{r}_i)^2\right]. \end{aligned} \quad (2.9)$$

For n fermions, the anti-symmetric free propagator $e_{\mathcal{A}}^{-\epsilon\hat{T}}$ in D dimension is given by the determinant

$$G_0(\mathbf{x}', \mathbf{x}, \epsilon) = \langle \mathbf{x}' | e_{\mathcal{A}}^{-\epsilon\hat{T}} | \mathbf{x} \rangle$$

$$= \frac{1}{n!} \det \left(\frac{1}{(2\pi\epsilon)^{D/2}} \exp \left[-\frac{1}{2\epsilon} (\mathbf{r}'_i - \mathbf{r}_j)^2 \right] \right) \quad (2.10)$$

$$= \frac{1}{n!} \sum_p (-1)^P g_0(\mathbf{x}'_p, \mathbf{x}, \epsilon) \quad (2.11)$$

$$= \frac{1}{n!} \sum_p (-1)^P g_0(\mathbf{x}', \mathbf{x}_p, \epsilon) \quad (2.12)$$

where \mathbf{x}_p is a particle permutation of \mathbf{x} with $P = 0$ for even permutations and $P = 1$ for odd permutations. From from (2.10), $G_0(\mathbf{x}', \mathbf{x}, \epsilon)$ is antisymmetric in \mathbf{x}' and in \mathbf{x} .

The contraction of two free fermion propagators gives

$$\begin{aligned} \langle \mathbf{x}' | e_{\mathcal{A}}^{-a\hat{T}} e^{-b\hat{V}} e_{\mathcal{A}}^{-c\hat{T}} | \mathbf{x}^* \rangle &= \int d\mathbf{x} G_0(\mathbf{x}', \mathbf{x}, a) e^{-b\frac{1}{2}\mathbf{x}^2} G_0(\mathbf{x}, \mathbf{x}^*, c) \\ &= \frac{1}{(n!)^2} \sum_{p,q} (-1)^{P+Q} \int d\mathbf{x} g_0(\mathbf{x}'_p, \mathbf{x}, a) e^{-b\frac{1}{2}\mathbf{x}^2} g_0(\mathbf{x}, \mathbf{x}_q^*, c) \\ &= \frac{1}{(n!)^2} \sum_{p,q} (-1)^{P+Q} \langle \mathbf{x}' | e^{-a\hat{T}} e^{-b\hat{V}} e^{-c\hat{T}} | \mathbf{x}^* \rangle. \end{aligned} \quad (2.13)$$

Since the contraction holds for the n -particle free propagator, the above is just

$$\begin{aligned} \langle \mathbf{x}' | e_{\mathcal{A}}^{-a\hat{T}} e^{-b\hat{V}} e_{\mathcal{A}}^{-c\hat{T}} | \mathbf{x}^* \rangle &= e^{-\nu\frac{1}{2}\mathbf{x}'^2 - \mu\frac{1}{2}\mathbf{x}^{*2}} \frac{1}{(n!)^2} \sum_{p,q} (-1)^{P+Q} g_0(\mathbf{x}'_p, \mathbf{x}_q^*, \kappa) \\ &= e^{-\nu\frac{1}{2}\mathbf{x}'^2 - \mu\frac{1}{2}\mathbf{x}^{*2}} \frac{1}{n!} \sum_p (-1)^P G_0(\mathbf{x}'_p, \mathbf{x}^*, \kappa). \end{aligned} \quad (2.14)$$

From (2.10), any row permutation changes the sign according to

$$G_0(\mathbf{x}'_p, \mathbf{x}, \epsilon) = (-1)^P G_0(\mathbf{x}', \mathbf{x}, \epsilon). \quad (2.15)$$

Hence

$$\begin{aligned} \langle \mathbf{x}' | e_{\mathcal{A}}^{-a\hat{T}} e^{-b\hat{V}} e_{\mathcal{A}}^{-c\hat{T}} | \mathbf{x}^* \rangle &= e^{-\nu\frac{1}{2}\mathbf{x}'^2 - \mu\frac{1}{2}\mathbf{x}^{*2}} G_0(\mathbf{x}', \mathbf{x}^*, \kappa) \\ &= \langle \mathbf{x}' | e^{-\nu\hat{V}} e_{\mathcal{A}}^{-\kappa\hat{T}} e^{-\mu\hat{V}} | \mathbf{x}^* \rangle. \end{aligned} \quad (2.16)$$

Thus we have shown that the operator contraction identity applies equally to free propagators of any number of harmonic fermions in any dimension. This immediately implies that:

- Since the sign of $G_0(\mathbf{x}', \mathbf{x}^*, \kappa)$ depends only on permutations of particle positions and *not* on κ , and contractions only change κ , the nodal structure of the free fermion propagator is preserved under all contractions. Hence, the discrete path integral for non-interacting harmonic fermions at any imaginary time-step has the *same* nodal structure as the free fermion propagator.

b) For fermions confined by a general potential $V(\mathbf{x})$, one can approximate

$$e^{-bV(\mathbf{x})} = \sum_k c_k e^{-b_k \mathbf{x}^2} \quad (2.17)$$

by a sum of Gaussians. The contraction then spawns multiple determinant propagators via

$$\int d\mathbf{x} G_0(\mathbf{x}', \mathbf{x}, a) e^{-bV(\mathbf{x})} G_0(\mathbf{x}, \mathbf{x}^*, c) = \sum_k c_k e^{-\nu_k \frac{1}{2} \mathbf{x}'^2} G_0(\mathbf{x}', \mathbf{x}^*, \kappa_k) e^{-\mu_k \frac{1}{2} \mathbf{x}^{*2}}, \quad (2.18)$$

and changes the nodal structure of the discrete path integral away from that of the free propagator.

c) This contraction holds true for the determinant free fermion propagator (2.10) but is not true when one only samples permutations randomly in (2.11) or (2.12). Therefore, doing fermion PIMC via *permutation sampling*^{17,18} will not precisely reproduce analytical results presented in this work.

Point a) explains why non-interacting harmonic fermions are as simple as free fermions. Point b) explains how generally interacting fermions are complicated by multiple determinants. Point c) explains that the use of the determinant propagator, while computationally more intensive, is superior to permutation sampling. This last point is related to an old finding by Lyubartsev¹⁸, that while there is no sign problem for 1D fermions when using the anti-symmetric propagator, there remains a low-level sign problem if one only does permutation sampling¹³. This work only uses the above anti-symmetric determinant free fermion propagator as originally employed by Takahashi and Imada¹² and subsequent authors^{9,10,13,18}.

III. THE UNIVERSAL DISCRETE PROPAGATOR OF HARMONIC PIMC

Because of the contraction identity (2.16), any left-right symmetric short-time operator of the form

$$\hat{G}_1(\epsilon) = \prod_i e_{\mathcal{A}}^{-a_i \epsilon \hat{T}} e^{-b_i \epsilon \hat{V}}, \quad (3.1)$$

can be contracted down to a single \hat{T} -operator form

$$\hat{G}_1(\epsilon) = e^{-\mu_1 \hat{V}} e_{\mathcal{A}}^{-\kappa_1 \hat{T}} e^{-\mu_1 \hat{V}}, \quad (3.2)$$

where μ_1 and κ_1 are functions of a_i , b_i , ϵ and whose matrix element

$$G_1(\mathbf{x}', \mathbf{x}, \epsilon) = \langle \mathbf{x}' | \hat{G}_1(\epsilon) | \mathbf{x} \rangle = e^{-\mu_1 \frac{1}{2} \mathbf{x}'^2} G_0(\mathbf{x}', \mathbf{x}, \kappa_1) e^{-\mu_1 \frac{1}{2} \mathbf{x}^2} \quad (3.3)$$

is the anti-symmetric, determinant short-time propagator. Since the the operator (3.2) is trivially related to its matrix element (3.3), the propagator, we will use words “operator” and “propagator” intechangably. For the well-known second-order Primitive Approximation (PA) propagator, $\mu_1 = \epsilon/2$ and $\kappa_1 = \epsilon$.

Following the same steps as in Ref.14, the contraction of N short-time fermion propagator $\hat{G}_1(\epsilon)$ gives the discrete PIMC operator at $\tau = N\epsilon$

$$\hat{G}_N = [\hat{G}_1(\epsilon)]^N = e^{-\mu_N \hat{V}} e_{\mathcal{A}}^{-\kappa_N \hat{T}} e^{-\mu_N \hat{V}}, \quad (3.4)$$

with *universal* coefficients

$$\zeta_N = \cosh(Nu), \quad (3.5)$$

$$\kappa_N = \frac{1}{\gamma} \sinh(Nu), \quad (3.6)$$

$$\mu_N = \frac{\zeta_N(Nu) - 1}{\kappa_N(Nu)} = \gamma \tanh(Nu/2). \quad (3.7)$$

Given κ_1 and μ_1 corresponding to $N = 1$, the above equations defines the N time-step PIMC propagator (3.4) analytically. In particular, (3.7) defines $\zeta_1 = 1 + \kappa_1 \mu_1$ from which the *portal* parameter u can be deduced from (3.5)

$$u = \cosh^{-1}(\zeta_1) = \ln \left(\zeta_1(\epsilon) + \sqrt{\zeta_1^2(\epsilon) - 1} \right). \quad (3.8)$$

The coefficient γ , defined at $N = 1$ by (3.6), remains unchanged for all N :

$$\gamma = \frac{\sinh(u)}{\kappa_1} = \frac{\sqrt{\zeta_1^2 - 1}}{\kappa_1} = \frac{\sqrt{\zeta_N^2 - 1}}{\kappa_N}. \quad (3.9)$$

The discrete PIMC propagator (3.4) is a universal function of the portal parameter u for *all* short-time propagators. Each short-time propagator only changes u through ζ_1 via (3.8).

For PA, $\zeta_1 = 1 + \epsilon^2/2$. In the continuum limit of $\epsilon = \tau/N \rightarrow 0$ with τ fixed,

$$u = \cosh^{-1}(\zeta_1) \rightarrow \epsilon - \frac{1}{24} \epsilon^3 + \dots \quad (3.10)$$

$$Nu \rightarrow N\epsilon = \tau, \quad \gamma = \sqrt{1 + \epsilon^2/4} \rightarrow 1 \quad (3.11)$$

and the PIMC propagator (3.4) becomes the exact n -harmonic-fermion propagator with

$$\kappa_N \rightarrow \sinh(\tau), \quad (3.12)$$

$$\mu_N \rightarrow \frac{\cosh(\tau) - 1}{\sinh(\tau)}. \quad (3.13)$$

That this exact propagator gives the correct ground state energy for up to 100 spin-polarized free fermions in a 2D harmonic oscillator has been shown previously in Ref.9. The above discussion can be regarded as its algorithmic derivation directly from PA.

IV. DISCRETE FERMION PARTITION FUNCTIONS

The partition function at $\tau = N\epsilon$ for n fermion is given by

$$\begin{aligned} Z_n(\tau) &= \int d\mathbf{x} G_N(\mathbf{x}, \mathbf{x}, \epsilon) \\ &= \frac{1}{n!} \frac{1}{(2\pi\kappa_N)^{nD/2}} \int d\mathbf{x} e^{-\mu_N \mathbf{x}^2} \det \left(\exp \left[-\frac{1}{2\kappa_N} (\mathbf{r}_i - \mathbf{r}_j)^2 \right] \right) \end{aligned} \quad (4.1)$$

For $n = 1$, one has

$$\begin{aligned} Z_1 &= \frac{1}{(2\pi\kappa_N)^{D/2}} \int d\mathbf{r}_1 e^{-\mu_N \mathbf{r}_1^2} = \frac{1}{(2\pi\kappa_N)^{D/2}} \left(\frac{\pi}{\mu_N} \right)^{D/2} \\ &= \left(\frac{1}{2(\zeta_N - 1)} \right)^{D/2} = \left(\frac{1}{2 \sinh(w/2)} \right)^D \end{aligned} \quad (4.2)$$

where we have defined

$$w = Nu. \quad (4.3)$$

This w is the algorithm's imaginary time, in contrast to the actual imaginary time of $\tau = N\epsilon$. They are equal in the continuum limit of $u \rightarrow \epsilon$.

For $n = 2$,

$$\begin{aligned} Z_2 &= \frac{1}{2!} \frac{1}{(2\pi\kappa_N)^{2D/2}} \int d\mathbf{x} e^{-\mu_N \mathbf{x}^2} \det \left(\exp \left[-\frac{1}{2\kappa_N} (\mathbf{r}_i - \mathbf{r}_j)^2 \right] \right) \\ &= \frac{1}{2!} \frac{1}{(2\pi\kappa_N)^{2D/2}} \int d\mathbf{r}_1 d\mathbf{r}_2 e^{-\mu_N (\mathbf{r}_1^2 + \mathbf{r}_2^2)} \begin{vmatrix} 1 & e_{12} \\ e_{21} & 1 \end{vmatrix} \end{aligned} \quad (4.4)$$

where we have defined

$$e_{ij} = \exp \left[-\frac{1}{2\kappa_N} (\mathbf{r}_i - \mathbf{r}_j)^2 \right]. \quad (4.5)$$

From Appendix A, one finds that

$$Z_2 = \frac{1}{2!}(z_1^2 - z_2), \quad (4.6)$$

where

$$\begin{aligned} z_n &= \frac{1}{(2 \sinh(nw/2))^D} = \left(\frac{1}{e^{nw/2} - e^{-nw/2}} \right)^D \\ &= \left(\frac{e^{-nw/2}}{1 - e^{-nw}} \right)^D = \left(\frac{b^{n/2}}{1 - b^n} \right)^D \end{aligned} \quad (4.7)$$

with $b = \exp(-w)$.

For $n = 3$, one has

$$\begin{aligned} Z_3 &= \frac{1}{3!} \frac{1}{(2\pi\kappa_N)^{3D/2}} \int d\mathbf{r}_1 d\mathbf{r}_2 d\mathbf{r}_3 e^{-\mu_N(\mathbf{r}_1^2 + \mathbf{r}_2^2 + \mathbf{r}_3^2)} \begin{vmatrix} 1 & e_{12} & e_{13} \\ e_{21} & 1 & e_{23} \\ e_{31} & e_{32} & 1 \end{vmatrix} \\ &= \frac{1}{3!} \frac{1}{(2\pi\kappa_N)^{3D/2}} \int d\mathbf{r}_1 d\mathbf{r}_2 d\mathbf{r}_3 e^{-\mu_N(\mathbf{r}_1^2 + \mathbf{r}_2^2 + \mathbf{r}_3^2)} (1 - 3e_{12}e_{21} + 2e_{12}e_{23}e_{31}) \end{aligned} \quad (4.8)$$

Again, from Appendix A,

$$Z_3 = \frac{1}{3!}(z_1^3 - 3z_2z_1 + 2z_3). \quad (4.9)$$

Similarly one can show that for $n = 4$,

$$Z_4 = \frac{1}{4!}(z_1^4 - 6z_2z_1^2 + 3z_2^2 + 8z_3z_1 - 6z_4). \quad (4.10)$$

It has been known for sometime that the free fermion partition Z_n in the *continuum* limit of $w \rightarrow \tau$ is given by¹⁹:

$$Z_n = \frac{1}{n!} \begin{vmatrix} z_1 & 1 & 0 & 0 & \cdots \\ z_2 & z_1 & 2 & 0 & \cdots \\ z_3 & z_2 & z_1 & 3 & \cdots \\ z_4 & z_3 & z_2 & z_1 & \cdots \\ \vdots & \vdots & \vdots & \vdots & \cdots \end{vmatrix} \quad (4.11)$$

and obeys the recursion^{19,20}:

$$Z_n = \frac{1}{n} \sum_{i=1}^n (-1)^{i-1} z_i Z_{n-i} \quad (4.12)$$

with $Z_0 = 1$. By generalizing (4.4) to the case of a $n \times n$ determinant, Chaudhary²¹ has shown that the n -fermion *discrete* PIMC partition functions at *every* N^{th} time-step, such as (4.6), (4.9), (4.10), obey the same recursion relation (4.12) and therefore also given by the same determinant form (4.11). Since the discrete partition function (4.1) contains the continuum limit as its special case, the above can be viewed as an alternative derivation of the fermion recursion relation directly from the path integral formalism.

V. ANALYTICAL THERMODYNAMIC AND HAMILTONIAN ENERGIES

To compute the discrete PIMC thermodynamic energy at $\tau = N\epsilon$, note that the universal coefficients $\kappa(Nu)$ and $\mu(Nu)$ are functions of the algorithm imaginary time $w = Nu$. Therefore, one can write

$$\begin{aligned} E_n^T(\tau) &= -\frac{\partial \log Z_n}{\partial \tau} = \frac{\partial w}{\partial \tau} \left(-\frac{\partial \log Z_n}{\partial w} \right), \\ &= \rho_T(\epsilon) E_n(w). \end{aligned} \quad (5.1)$$

where ρ_T is the same prefactor for all n -fermion energy from (3.8)

$$\rho_T(\epsilon) = \frac{\partial w}{\partial \tau} = \frac{du}{d\epsilon} = \frac{1}{\sqrt{\zeta_1^2 - 1}} \frac{d\zeta_1}{d\epsilon}. \quad (5.2)$$

Since the basic partition function z_n (4.7) depends on w only through $b = e^{-w}$, one has the universal discrete N^{th} time-step thermodynamic energy

$$\begin{aligned} E_n(w) &= -\frac{\partial \log Z_n(b)}{\partial b} \frac{\partial b}{\partial w} \\ &= b \frac{\partial \log Z_n(b)}{\partial b} \end{aligned} \quad (5.3)$$

for all short-time propagators. Each short-time propagator only modifies its argument w via u .

For later comparisons, we will now only consider the case of $D = 2$. For $D = 2$, the n -particle partition function is particularly simple:

$$z_n(b) = \frac{b^n}{(1 - b^n)^2}. \quad (5.4)$$

For one fermion, $\log Z_1 = \log b - 2 \log(1 - b)$ and (5.3) gives

$$E_1(w) = (1 + 2 \frac{b}{1 - b}) = \coth(w/2) = \frac{\sinh(w)}{\cosh(w) - 1}. \quad (5.5)$$

For two fermions,

$$Z_2(w) = z_1^2(w) - z_2(w) = \frac{4b^3}{(1-b)^4(1+b)^2} \quad (5.6)$$

$$E_2(w) = \frac{3+2b+3b^2}{1-b^2} = \frac{1+3\cosh(w)}{\sinh(w)}. \quad (5.7)$$

For three fermions

$$Z_3(w) = z_1^3 - 3z_1z_2 + 2z_3 = \frac{6b^5(b^2+4b+1)}{(1-b)^6(1+b)^2(1+b+b^2)}, \quad (5.8)$$

$$\begin{aligned} E_3(w) &= \frac{5+31b+47b^2+50b^3+47b^4+31b^5+5b^6}{1+5b+5b^2-5b^4-5b^5-b^6} \\ &= \frac{25+47\cosh(w)+31\cosh(2w)+5\cosh(3w)}{5\sinh(w)+5\sinh(2w)+\sinh(3w)} \end{aligned} \quad (5.9)$$

For $n = 4, 5, 6, 10$, the lengthy expressions for the discrete energy are given in Appendix B.

The fastest numerical method of computing the thermodynamic energy (5.1) at imaginary time $\tau = N\epsilon$, corresponding to contracting (integrating over) N short-time propagator $G_1(\epsilon)$, is to determine u from (3.8), evaluate the discrete energy $E_n(w)$ and multiply it by the prefactor $\rho_T(\tau/N)$. However, in order to determine $E_n(w)$ analytically, one must also perform the subtractions in $Z_n(w)$, as in (5.6) and (5.8) analytically, otherwise their direct numerical evaluations at $n > 3$ would quickly exhaust machine-precision.

For n and N small, one can obtain analytical expressions for $E_n^T(\tau)$. Instead of (3.8), one observes that

$$e^u = \zeta_1 + \sqrt{\zeta_1^2 - 1} \quad \text{and} \quad e^{-u} = \zeta_1 - \sqrt{\zeta_1^2 - 1}. \quad (5.10)$$

For $n = 2$, (5.7) gives

$$\begin{aligned} E_2(Nu) &= \frac{2+3[e^{Nu}+e^{-Nu}]}{[e^{Nu}-e^{-Nu}]} \\ &= \frac{2+3[(\zeta_1+\sqrt{\zeta_1^2-1})^N+(\zeta_1-\sqrt{\zeta_1^2-1})^N]}{[(\zeta_1+\sqrt{\zeta_1^2-1})^N-(\zeta_1-\sqrt{\zeta_1^2-1})^N]}. \end{aligned} \quad (5.11)$$

For $N = 2$,

$$E_2^T(2u) = E_2(2u) \frac{d\zeta_1}{d\epsilon} = \frac{3\zeta_1^2-1}{\zeta_1(\zeta_1^2-1)} \frac{d\zeta_1}{d\epsilon}. \quad (5.12)$$

The RHS are functions of ϵ through $\zeta_1(\epsilon)$. For PA, $\zeta_1 = 1 + \epsilon^2/2$ and $d\zeta_1/d\epsilon = \epsilon$, the two-bead ($N = 2$) thermodynamic energy in terms of $\tau = 2\epsilon$ is then

$$E_2^T(2u) = \frac{4}{\tau} \frac{(1 + \frac{3}{8}\tau^2 + \frac{3}{128}\tau^4)}{(1 + \frac{3}{16}\tau^2 + \frac{1}{128}\tau^4)}. \quad (5.13)$$

Similarly, one can determine the 3- and 4-bead two-fermion energies:

$$\begin{aligned} E_2^T(3u) &= \frac{4}{\tau} \frac{(1 + \frac{3}{8}\tau^2 + \frac{1}{36}\tau^4 + \frac{1}{1944}\tau^6)}{(1 + \frac{1}{9}\tau^2)(1 + \frac{1}{27}\tau^2)(1 + \frac{1}{36}\tau^2)}, \\ E_2^T(4u) &= \frac{4}{\tau} \frac{(1 + \frac{3}{8}\tau^2 + \frac{15}{512}\tau^4 + \frac{3}{4096}\tau^6) + \frac{3}{524288}\tau^8}{(1 + \frac{1}{32}\tau^2)(1 + \frac{1}{64}\tau^2)(1 + \frac{1}{8}\tau^2 + \frac{1}{512}\tau^4)}. \end{aligned} \quad (5.14)$$

Despite the appearance of exponentials in (5.7), because of (5.10), all discrete energies are just rational functions of τ .

As shown in Ref.15, for the 1D harmonic oscillator, the Hamiltonian energy is given similarly as the thermodynamic energy (5.1), but with a different prefactor:

$$E_n^H(\tau) = \rho_H(\epsilon) E_n(w). \quad (5.15)$$

where

$$\rho_H(\epsilon) = \frac{1}{2} \left(\gamma(\epsilon) + \frac{1}{\gamma(\epsilon)} \right), \quad (5.16)$$

with $\gamma(\epsilon)$ given by (3.9).

The ratio of the two energies at any discrete N time step is therefore given by

$$\frac{E_n^H(Nu)}{E_n^T(Nu)} = \frac{\rho_H(\epsilon)}{\rho_T(\epsilon)} \quad (5.17)$$

and is solely determined by the short-time propagator.

For PA, this ratio is just $(1 + \epsilon^2/8)$, giving the discrete Hamiltonian energies as

$$E_n^H(Nu) = \left[1 + \frac{1}{8} \left(\frac{\tau}{N} \right)^2 \right] E_n^T(Nu). \quad (5.18)$$

Since the harmonic oscillator is separable, the above is true for any number of particles in any dimension, for all permutations, and therefore for fermions.

In Fig.2, PA's thermodynamic and Hamiltonian energies for two, three, four and six fermions, up to $N = 8$, as determined above analytically, are compared with direct PIMC simulations. The agreements are perfect.

Fig.2 also illustrates that, at these small N values, PA's thermodynamic energy showed no convergence whatsoever toward the exact ground state fermion energies. By contrast, the energy minimum of the Hamiltonian energy is already close to that of the ground state by $N = 8$. As explained in Ref.15, the thermodynamic energy converges to the same order as the short-time propagator, but the Hamiltonian energy converges at twice the order of the algorithm and is everywhere an upper bound to the ground state energy.

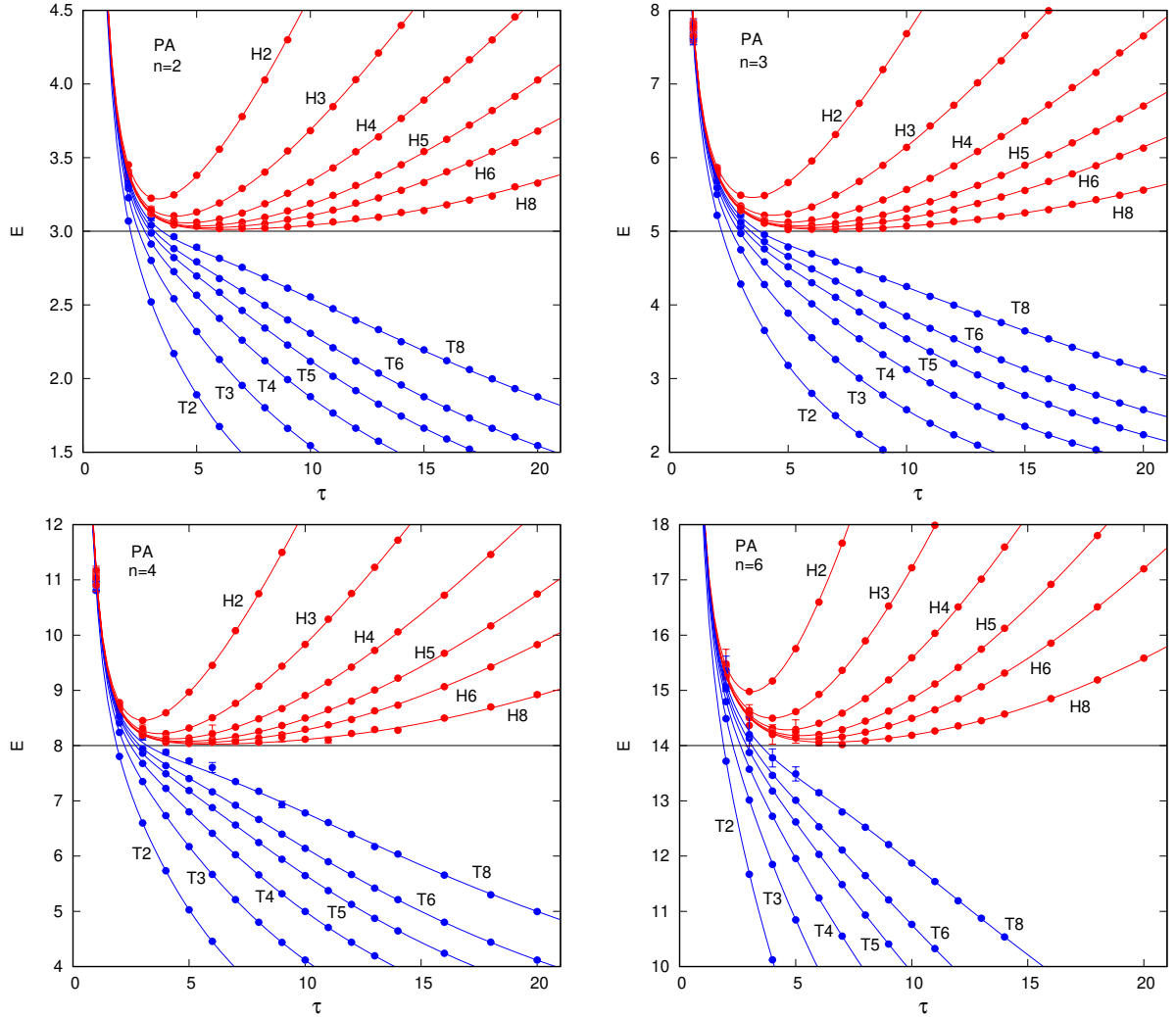


FIG. 2: (color online) The PA propagator's non-interacting 2, 3, 4 and 6-fermion N -bead thermodynamic and Hamiltonian energies in a 2D harmonic oscillator, denoted by TN and HN , are plotted as a function of the imaginary time $\tau = N\epsilon$. The data points are PIMC calculations and smooth curves are analytical results from (5.1) and (5.15).

This means that if one uses fourth-order propagators, then the Hamiltonian energy will converge to the eighth-order. Using the fourth-order algorithm BB3 as summarized in Appendix C, with only three beads (three free fermion propagators), one can obtain the exact ground state energy of up to 28 non-interacting fermions as shown in Fig.3. For $n = 6$, since $E_6(w)$ is known analytically from Appendix B, one can also compute its energy curves numerically, in also perfect agreement with PIMC data. For parameter values $t_1 = 0.26, 0.25, 0.24$, the minimum Hamiltonian energies can be determined numerically to be 14.003, 14.0003

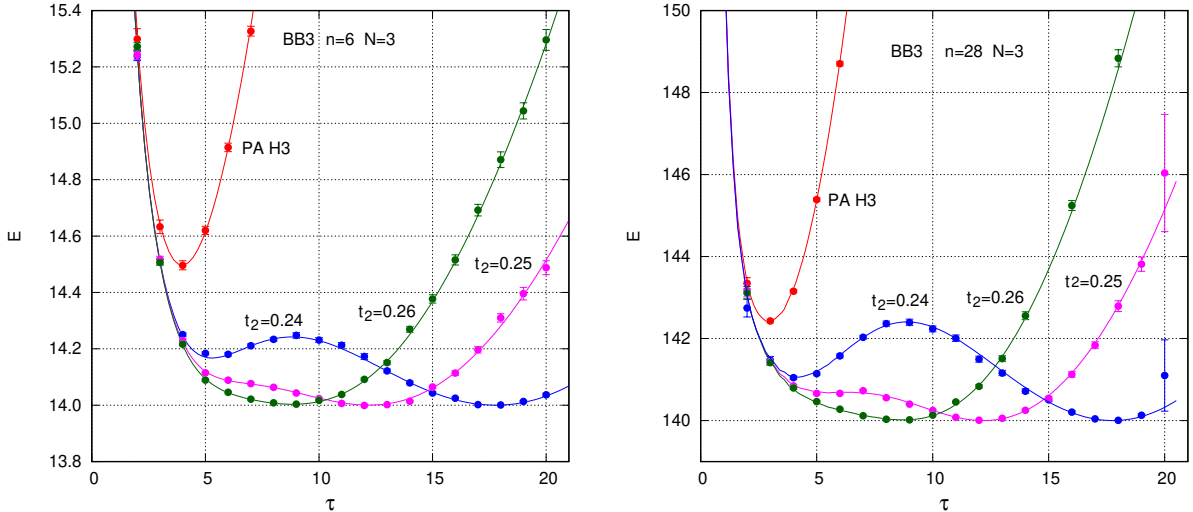


FIG. 3: (color online) The Hamiltonian energies of the fourth-order Best 3-Bead (BB3) algorithm in solving for the ground state energy of 6 and 28 non-interacting fermions in a 2D harmonic oscillator. Notice that two energy minima are possible for $t_2 = 0.24$.

and 14.00002 respectively. For $n = 28$, given the complexity already shown by $E_{10}(w)$ in Appendix B, $E_{28}(w)$ is too lengthy to be derived analytically. However, since $E_{28}(\tau)$ is just the energy of 28 non-interacting harmonic fermions, it can be numerically computed via PIMC using the exact continuum propagator in only two beads, without any sign problem. Interpolate some 50 discrete values of $E_{28}(\tau)$ then produces the smooth energy curves as shown in Fig.3. The sudden appearance of large error bars at $\tau = 20$ is not due the sign problem nor limited Monte Carlo samplings. It is because for $n = 28$ at such a large τ , the determinant of the propagator matrix is too near zero and the matrix cannot be reliably inverted using double precision arithmetic. This error plagues all large n calculations at large τ , but would not appear if the code can be executed with greater arithmetic precision.

For non-interacting closed-shell fermions then, the ground state energy can be extracted by optimizing the Hamiltonian energy using this BB3 propagator, with seemingly no sign problem for up to about 30 fermions.

VI. THE FERMION PIMC SIGN PROBLEM

Because the operator contraction is exact, there is no sign problem in the analytical calculations in the last section. All energies are just rational functions of τ . In PIMC

simulations, the partition function at $\tau = N\epsilon$ is a discrete path integral of N short-time determinant propagators G_1 given by (3.3):

$$Z = \int d\mathbf{x}_1 \cdots d\mathbf{x}_N G_1(\mathbf{x}_1, \mathbf{x}_2; \epsilon) G_1(\mathbf{x}_2, \mathbf{x}_3; \epsilon) \cdots G_1(\mathbf{x}_N, \mathbf{x}_1; \epsilon). \quad (6.1)$$

Since the product of determinants is not necessary positive, one decomposes the integrand into its overall sign and absolute value,

$$\begin{aligned} G_1(\mathbf{x}_1, \mathbf{x}_2; \epsilon) \cdots G_1(\mathbf{x}_N, \mathbf{x}_1; \epsilon) &= \text{sgn} |G_1(\mathbf{x}_1, \mathbf{x}_2; \epsilon) \cdots G_1(\mathbf{x}_N, \mathbf{x}_1; \epsilon)| \\ &= \text{sgn} P(\mathbf{x}_1, \cdots, \mathbf{x}_N). \end{aligned} \quad (6.2)$$

Any observable $\mathcal{O}(\mathbf{x})$ can then be computed as

$$\begin{aligned} \langle \mathcal{O} \rangle &= \frac{\int d\mathbf{x}_1 \cdots d\mathbf{x}_N \bar{\mathcal{O}} \text{sgn} P(\mathbf{x}_1, \cdots, \mathbf{x}_N)}{\int d\mathbf{x}_1 \cdots d\mathbf{x}_N \text{sgn} P(\mathbf{x}_1, \cdots, \mathbf{x}_N)} \\ &= \frac{\int d\mathbf{x}_1 \cdots d\mathbf{x}_N \bar{\mathcal{O}} \text{sgn} P(\mathbf{x}_1, \cdots, \mathbf{x}_N) / \int d\mathbf{x}_1 \cdots d\mathbf{x}_N P(\mathbf{x}_1, \cdots, \mathbf{x}_N)}{\int d\mathbf{x}_1 \cdots d\mathbf{x}_N \text{sgn} P(\mathbf{x}_1, \cdots, \mathbf{x}_N) / \int d\mathbf{x}_1 \cdots d\mathbf{x}_N P(\mathbf{x}_1, \cdots, \mathbf{x}_N)} \\ &= \frac{\langle \bar{\mathcal{O}} \text{sgn} \rangle_P}{\langle \text{sgn} \rangle_P}, \end{aligned} \quad (6.3)$$

where $\bar{\mathcal{O}}$ is the operator averaged over each short-time propagator (the bead-average)

$$\bar{\mathcal{O}} = \frac{1}{N} \sum_{i=1}^N \mathcal{O}(\mathbf{x}_i). \quad (6.4)$$

Both the numerator and denominator of (6.3) can be computed by the Monte Carlo method because $P(\mathbf{x}_1, \cdots, \mathbf{x}_N)$ is non-negative. The sign problem arises only when the average sign $s = \langle \text{sgn} \rangle_P \rightarrow 0$ such that (6.3) can no longer be evaluated with stability.

The average sign values for the 2, 3, 4 and 6-fermion calculation in Fig.2 are shown on Fig.4. For up to $N = 8$, the average sign is nowhere near zero. This is why the energy calculations in Fig.2 (and Fig.3) are without problem. However, there are at least two surprises in Fig.4: 1) It is generally expected that s should deceases exponentially^{22,23} with increasing n and N . In the 2 and 4-fermion cases, it was unexpected to find that s actually levels off to a constant value at large τ . The predicted s values for the two-fermion case are derived in Appendix D. This was not noticed before because most calculations²³ were done at $\tau \ll 10$. 2) More surprisingly, for $n = 3$ and 6, the average sign does not decrease monotonically, but reaches a sign minimum then reverts back to 1 at large τ . Since $n = 3$ and 6 are a closed-shell harmonic states in 2D, this immediately suggests that one should check whether this is true for all closed-shell fermion states.

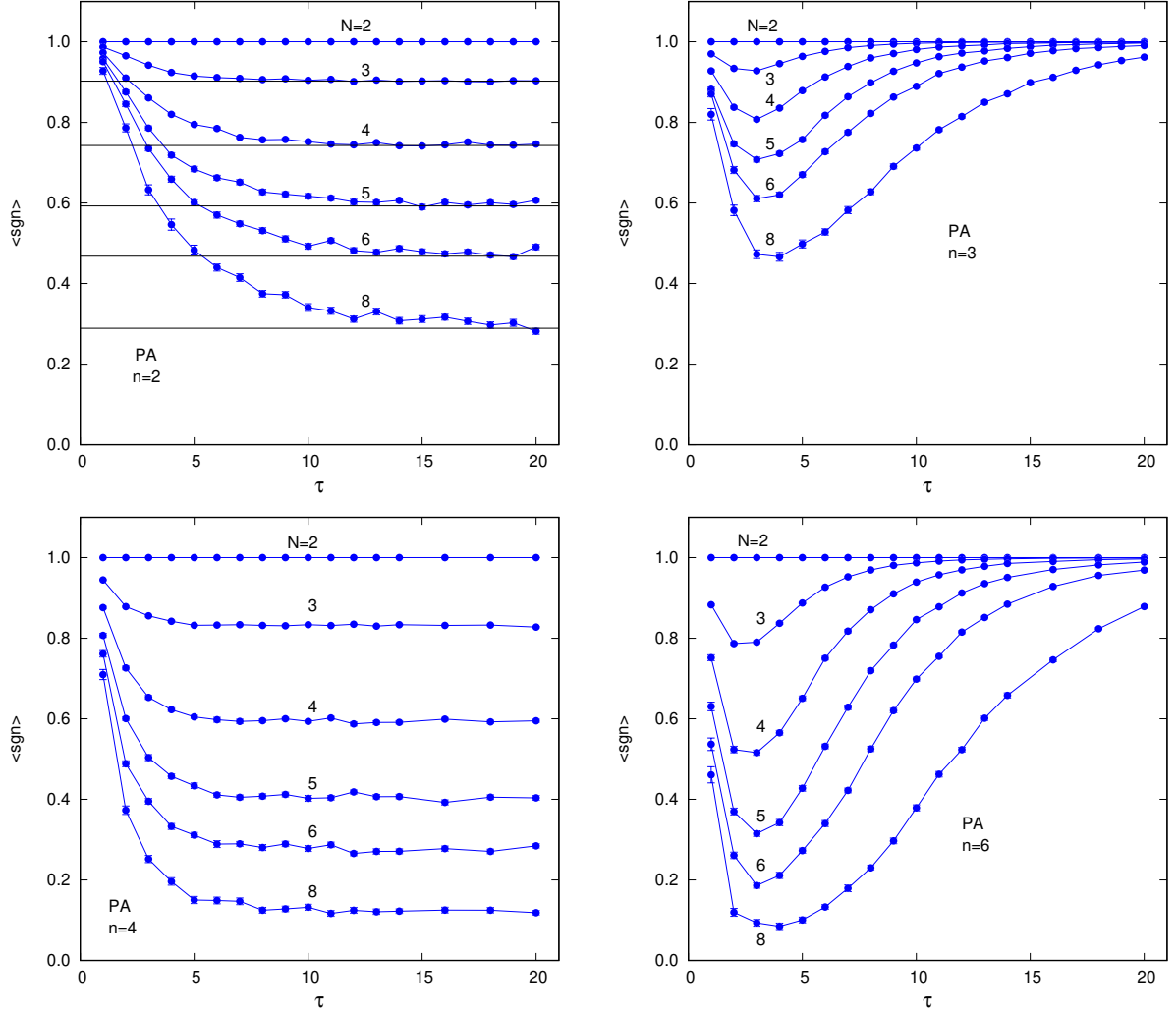


FIG. 4: (color online) The PA propagator's average sign $\langle \text{sgn} \rangle$ for $n = 2, 3, 4, 6$ non-interacting harmonic fermions at various bead number N as a function of τ . The horizontal black lines in the two-fermion case are average sign values at large τ deduced in Appendix D.

This is indeed the case for both 2D and 3D as shown in Fig.5. One observes that at $\tau = 1$, in both 2D and 3D, s decreases with increasing n , which is the conventional understanding^{22,23}. However, Fig.5 clearly shows that this is not the case for closed-shell states at large τ .

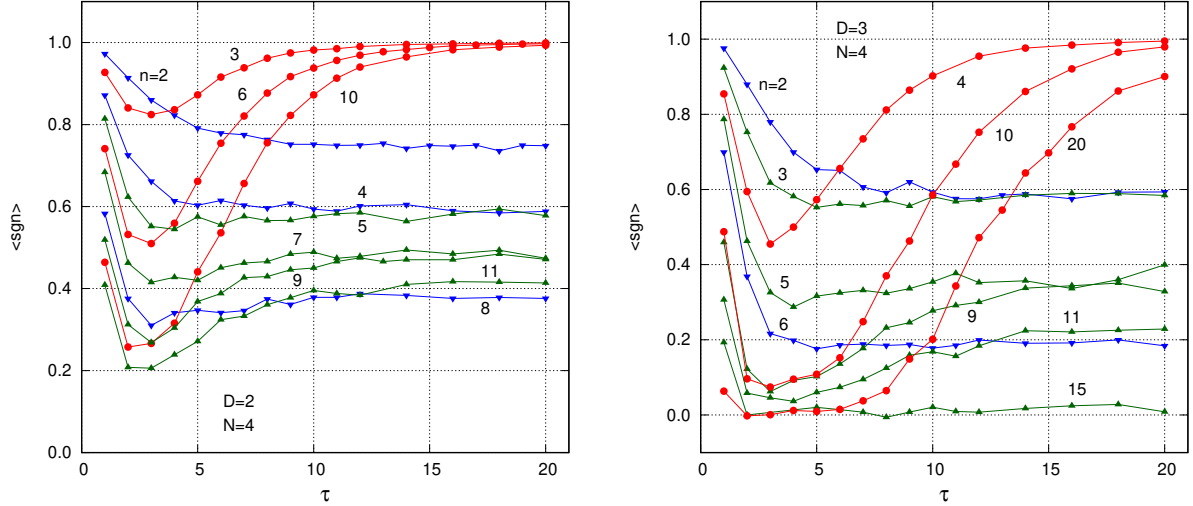


FIG. 5: (color online) The average sign of a $N = 4$ bead calculation in 2D and 3D for various n non-interacting harmonic fermions. The average sign reverts back to one for closed-shell number of fermions in the large τ limit.

VII. WHY NO SIGN PROBLEM FOR CLOSED-SHELL STATES?

For harmonic fermions in more than one dimension, because of the energy level degeneracy, there are closed-shell states when fermions completely filled up to the highest degenerate level. In one dimension, because there is no degeneracy, every occupied state is a closed-shell state. The surprising reason why there is no sign problem in closed-shell states, is the same reason why there is no sign problem for fermions in one dimension¹³; they are all closed-shell states. The only difference is that in one dimension, there is no sign problem at all τ . In more than one dimension, that is true only at large τ .

Let's explain this with increasing dimension. From (2.10), the two-fermion free propagator in 2D is given by

$$G_0(\mathbf{r}'_1, \mathbf{r}'_2, \mathbf{r}_1, \mathbf{r}_2; \epsilon) = \frac{1}{2} \frac{1}{(2\pi\epsilon)^2} \det \begin{pmatrix} e^{-(\mathbf{r}'_1 - \mathbf{r}_1)^2/(2\epsilon)} & e^{-(\mathbf{r}'_1 - \mathbf{r}_2)^2/(2\epsilon)} \\ e^{-(\mathbf{r}'_2 - \mathbf{r}_1)^2/(2\epsilon)} & e^{-(\mathbf{r}'_2 - \mathbf{r}_2)^2/(2\epsilon)} \end{pmatrix}, \quad (7.1)$$

$$= \frac{1}{2} \frac{1}{(2\pi\epsilon)^2} e^{-\frac{1}{2\epsilon}[(\mathbf{r}'_1 - \mathbf{r}_1)^2 + (\mathbf{r}'_2 - \mathbf{r}_2)^2]} \left(1 - e^{-\frac{1}{\epsilon} \mathbf{r}'_{21} \cdot \mathbf{r}_{21}}\right), \quad (7.2)$$

where $\mathbf{r}'_{21} = \mathbf{r}'_2 - \mathbf{r}'_1$ and $\mathbf{r}_{21} = \mathbf{r}_2 - \mathbf{r}_1$. Its sign is given by the sign of the round bracket above, which in turn is given by the sign of $\mathbf{r}'_{21} \cdot \mathbf{r}_{21}$. Therefore one has

$$\text{sgn}(G_0(\mathbf{r}'_1, \mathbf{r}'_2, \mathbf{r}_1, \mathbf{r}_2; \epsilon)) = \text{sgn}(\mathbf{r}'_{21} \cdot \mathbf{r}_{21}). \quad (7.3)$$

For a closed loop of three propagators,

$$\begin{aligned} \text{sgn}\left(G_0(\mathbf{r}_{21}, \mathbf{r}'_{21})G_0(\mathbf{r}'_{21}, \mathbf{r}''_{21})G_0(\mathbf{r}''_{21}, \mathbf{r}_{21})\right) &= \text{sgn}\left((\mathbf{r}_{21} \cdot \mathbf{r}'_{21})(\mathbf{r}'_{21} \cdot \mathbf{r}''_{21})(\mathbf{r}''_{21} \cdot \mathbf{r}_{21})\right), \\ &= |\mathbf{r}_{21}|^2 |\mathbf{r}'_{21}|^2 |\mathbf{r}''_{21}|^2 \text{sgn}(\cos \theta \cos \theta' \cos \theta''), \end{aligned} \quad (7.4)$$

one has the sign problem because the cosine functions resulting from the dot products can have both signs. However, at one dimension, there is no dot product, no cosine functions,

$$\begin{aligned} \text{sgn}\left(G_0(x_{21}, x'_{21})G_0(x'_{21}, x''_{21})G_0(x''_{21}, x_{21})\right) &= \text{sgn}\left((x_{21}x'_{21})(x'_{21}x''_{21})(x''_{21}x_{21})\right), \\ &= \text{sgn}\left((x_{21})^2 (x'_{21})^2 (x''_{21})^2\right) \geq 0, \end{aligned} \quad (7.5)$$

and therefore no sign problem. Note that x_{ij} can be viewed as a *signed-distance*. In general then, the sign of a loop of N two-fermion propagators is just the sign of a product of N *signed-distance squared*, which is non-negative.

To put it differently, a loop of N two-fermion propagators in any dimension other than one has a sign problem because the two-fermion state is never a closed-shell state except in one dimension.

Consider now the three-fermion free propagator from (2.10) with $\mathbf{s}_i \equiv \mathbf{r}'_i$,

$$G_0(\mathbf{s}_i, \mathbf{r}_i; \epsilon) \propto e^{-(\mathbf{s}_1^2 + \mathbf{s}_2^2 + \mathbf{s}_3^2 + \mathbf{r}_1^2 + \mathbf{r}_2^2 + \mathbf{r}_3^2)/(2\epsilon)} \det \begin{pmatrix} e^{\mathbf{s}_1 \cdot \mathbf{r}_1/\epsilon} & e^{\mathbf{s}_1 \cdot \mathbf{r}_2/\epsilon} & e^{\mathbf{s}_1 \cdot \mathbf{r}_3/\epsilon} \\ e^{\mathbf{s}_2 \cdot \mathbf{r}_1/\epsilon} & e^{\mathbf{s}_2 \cdot \mathbf{r}_2/\epsilon} & e^{\mathbf{s}_2 \cdot \mathbf{r}_3/\epsilon} \\ e^{\mathbf{s}_3 \cdot \mathbf{r}_1/\epsilon} & e^{\mathbf{s}_3 \cdot \mathbf{r}_2/\epsilon} & e^{\mathbf{s}_3 \cdot \mathbf{r}_3/\epsilon} \end{pmatrix}, \quad (7.6)$$

its sign is given by the determinant above. Multiply its first row by $e^{(\mathbf{s}_2 - \mathbf{s}_1) \cdot \mathbf{r}_1/\epsilon} \equiv e^{\mathbf{s}_{21} \cdot \mathbf{r}_1/\epsilon}$ and $e^{\mathbf{s}_{31} \cdot \mathbf{r}_1/\epsilon}$ and subtract them from the second and third row respectively gives

$$\begin{aligned} &\det \begin{pmatrix} e^{\mathbf{s}_1 \cdot \mathbf{r}_1/\epsilon} & e^{\mathbf{s}_1 \cdot \mathbf{r}_2/\epsilon} & e^{\mathbf{s}_1 \cdot \mathbf{r}_3/\epsilon} \\ 0 & e^{\mathbf{s}_2 \cdot \mathbf{r}_2/\epsilon} - e^{\mathbf{s}_1 \cdot \mathbf{r}_2/\epsilon + \mathbf{s}_{21} \cdot \mathbf{r}_1/\epsilon} & e^{\mathbf{s}_2 \cdot \mathbf{r}_3/\epsilon} - e^{\mathbf{s}_1 \cdot \mathbf{r}_3/\epsilon + \mathbf{s}_{21} \cdot \mathbf{r}_1/\epsilon} \\ 0 & e^{\mathbf{s}_3 \cdot \mathbf{r}_2/\epsilon} - e^{\mathbf{s}_1 \cdot \mathbf{r}_2/\epsilon + \mathbf{s}_{31} \cdot \mathbf{r}_1/\epsilon} & e^{\mathbf{s}_3 \cdot \mathbf{r}_3/\epsilon} - e^{\mathbf{s}_1 \cdot \mathbf{r}_3/\epsilon + \mathbf{s}_{31} \cdot \mathbf{r}_1/\epsilon} \end{pmatrix}, \\ &= e^{\mathbf{s}_1 \cdot \mathbf{r}_1/\epsilon} \det \begin{pmatrix} e^{\mathbf{s}_2 \cdot \mathbf{r}_2/\epsilon} (1 - e^{-\mathbf{s}_{21} \cdot \mathbf{r}_{21}/\epsilon}) & e^{\mathbf{s}_2 \cdot \mathbf{r}_3/\epsilon} (1 - e^{-\mathbf{s}_{21} \cdot \mathbf{r}_{31}/\epsilon}) \\ e^{\mathbf{s}_3 \cdot \mathbf{r}_2/\epsilon} (1 - e^{-\mathbf{s}_{31} \cdot \mathbf{r}_{21}/\epsilon}) & e^{\mathbf{s}_3 \cdot \mathbf{r}_3/\epsilon} (1 - e^{-\mathbf{s}_{31} \cdot \mathbf{r}_{31}/\epsilon}) \end{pmatrix}. \end{aligned} \quad (7.7)$$

In the limit of $\epsilon \rightarrow \infty$, to leading order in $1/\epsilon$, the sign of the above determinant is given by the expansion of each matrix element's bracket,

$$\det \begin{pmatrix} (\mathbf{s}_{21} \cdot \mathbf{r}_{21}) & (\mathbf{s}_{21} \cdot \mathbf{r}_{31}) \\ (\mathbf{s}_{31} \cdot \mathbf{r}_{21}) & (\mathbf{s}_{31} \cdot \mathbf{r}_{31}) \end{pmatrix} = (\mathbf{s}_{21} \cdot \mathbf{r}_{21})(\mathbf{s}_{31} \cdot \mathbf{r}_{31}) - (\mathbf{s}_{31} \cdot \mathbf{r}_{21})(\mathbf{s}_{21} \cdot \mathbf{r}_{31}), \quad (7.8)$$

$$= (\mathbf{s}_{21} \times \mathbf{s}_{31}) \cdot (\mathbf{r}_{21} \times \mathbf{r}_{31}). \quad (7.9)$$

In more than 2D, the dot product in (7.9) will result in a cosine function, yielding the sign problems for three and more three-fermion propagators. However, in 2D, the cross-product

$$(\mathbf{s}_{21} \times \mathbf{s}_{31}) \cdot (\mathbf{r}_{21} \times \mathbf{r}_{31}) \rightarrow (\mathbf{s}_{21} \times \mathbf{s}_{31})_z (\mathbf{r}_{21} \times \mathbf{r}_{31})_z \quad (7.10)$$

is only a product of z -component with no cosine function and therefore no sign problem. Note that the cross-product in 2D is a *signed-area*. Therefore, the sign of a loop of N three-fermion propagators in the large τ limit is just the sign of a product of N *signed-area squared*, which is also non-negative.

The generalization of the determinant in (7.8) to four-fermion is

$$\det \begin{pmatrix} (\mathbf{s}_{21} \cdot \mathbf{r}_{21}) & (\mathbf{s}_{21} \cdot \mathbf{r}_{31}) & (\mathbf{s}_{21} \cdot \mathbf{r}_{41}) \\ (\mathbf{s}_{31} \cdot \mathbf{r}_{21}) & (\mathbf{s}_{31} \cdot \mathbf{r}_{31}) & (\mathbf{s}_{31} \cdot \mathbf{r}_{41}) \\ (\mathbf{s}_{41} \cdot \mathbf{r}_{21}) & (\mathbf{s}_{41} \cdot \mathbf{r}_{31}) & (\mathbf{s}_{41} \cdot \mathbf{r}_{41}) \end{pmatrix}. \quad (7.11)$$

Since \mathbf{r}_i are arbitrary, setting $\mathbf{r}_{21} = (a_x, 0, 0)$, $\mathbf{r}_{31} = (0, b_y, 0)$ and $\mathbf{r}_{41} = (0, 0, c_z)$ gives

$$\det \begin{pmatrix} (\mathbf{s}_{21})_x & (\mathbf{s}_{21})_y & (\mathbf{s}_{21})_z \\ (\mathbf{s}_{31})_x & (\mathbf{s}_{31})_y & (\mathbf{s}_{31})_z \\ (\mathbf{s}_{41})_x & (\mathbf{s}_{41})_y & (\mathbf{s}_{41})_z \end{pmatrix} (a_x b_y c_z) = \mathbf{s}_{21} \cdot (\mathbf{s}_{31} \times \mathbf{s}_{41}) (a_x b_y c_z), \quad (7.12)$$

$$= [\mathbf{s}_{21} \cdot (\mathbf{s}_{31} \times \mathbf{s}_{41})] [\mathbf{r}_{21} \cdot (\mathbf{r}_{31} \times \mathbf{r}_{41})], \quad (7.13)$$

because $(a_x b_y c_z)$ is the triple product $\mathbf{r}_{21} \cdot (\mathbf{r}_{31} \times \mathbf{r}_{41})$ and the propagator must be symmetric with respect to \mathbf{s}_i and \mathbf{r}_i . In 3D, the triple-product is a *signed-volume*. Therefore the sign of a loop of N four-fermion propagators in the large τ limit is the sign of a product of N *signed-volume squared*, which is again non-negative. (In 2D, the triple-product vanishes, and the sign of the four-fermion propagator is then determined by the next order term in the expansion of $(1/\epsilon)$.)

For $D + 1$ fermions in a D -dimension harmonic oscillator, the construction (7.13) generalizes to a product of signed volumes formed by D non-degenerate vectors, whose squares are non-negative.

For larger closed-shell states, such as $n = 6$ in 2D, or $n = 10$ in 3D, the sign of the propagator at large τ must be similarly given by some signed hyper-volumes. Unfortunately the method used here is too crude to make out the shape of these volumes.

VIII. THE SIGN PROBLEM WITH INTERACTION

To see how interactions alter the sign problem, consider first the case of pairwise harmonic interaction. The use of the exact *continuum* path integral to study fermions with pairwise harmonic potential has been studied extensively by Brosens, Devreese and Lemmens^{24,25}. This work focuses instead, on understanding the sign problem at each *discrete* time step of PIMC. For completeness, we give below a succinct summary of the needed results.

The Fortran code for this work is written for a n -particle Hamiltonian with a general pairwise interaction $\lambda|\mathbf{r}_i - \mathbf{r}_j|^k$, so that by simply setting $k = 2, -1, -3$, the same PIMC code would generate results for the harmonic, Coulomb and dipolar interaction respectively. This means that, once the harmonic force case agrees with analytical results derived below, one can then be assured that the code is working properly for the other interactions.

For the harmonic pairwise interaction, one can write the Hamiltonian as

$$H = T + V = \frac{1}{2m} \sum_{i=1}^n \mathbf{p}_i^2 + \frac{1}{2} \sum_{i=1}^n \mathbf{r}_i^2 + \frac{1}{2} \lambda \sum_{i=1}^n \sum_{j=1}^n (\mathbf{r}_i - \mathbf{r}_j)^2 \quad (8.1)$$

with $m = 1$. Let \mathbf{R} be the center-of-mass (CM) vector and \mathbf{u}_i the position relative to \mathbf{R} :

$$\mathbf{R} = \frac{1}{n} \sum_{i=1}^n \mathbf{r}_i, \quad \mathbf{u}_i = \mathbf{r}_i - \mathbf{R}. \quad (8.2)$$

It then follows that $\sum_{i=1}^n \mathbf{u}_i = 0$ and

$$\begin{aligned} V &= \frac{1}{2} \sum_{i=1}^n (\mathbf{R} + \mathbf{u}_i)^2 + \frac{1}{2} \lambda \sum_{i=1}^n \sum_{j=1}^n (\mathbf{u}_i - \mathbf{u}_j)^2 \\ &= \frac{1}{2} (\sqrt{n} \mathbf{R})^2 + \frac{1}{2} (1 + 2n\lambda) \sum_{i=1}^n \mathbf{u}_i^2. \end{aligned} \quad (8.3)$$

Similarly, the CM momentum is ($M = n$)

$$\mathbf{P} = M \dot{\mathbf{R}} = M \frac{1}{n} \sum_{i=1}^n \dot{\mathbf{r}}_i = \sum_{i=1}^n \mathbf{p}_i, \quad (8.4)$$

and the relative to CM momentum \mathbf{s}_i

$$\mathbf{s}_i = m \dot{\mathbf{u}}_i = m \dot{\mathbf{r}}_i - m \dot{\mathbf{R}} = \mathbf{p}_i - \frac{1}{n} \mathbf{P} \quad (8.5)$$

also satisfies

$$\sum_{i=1}^n \mathbf{s}_i = 0, \quad (8.6)$$

giving the kinetic energy as

$$T = \frac{1}{2} \sum_{i=1}^n \left(\frac{1}{n} \mathbf{P} + \mathbf{s}_i \right)^2 = \frac{1}{2n} \mathbf{P}^2 + \frac{1}{2} \sum_{i=1}^n \mathbf{s}_i^2. \quad (8.7)$$

The total Hamiltonian is then

$$H = \frac{1}{2n} \mathbf{P}^2 + \frac{1}{2} n \mathbf{R}^2 + \frac{1}{2} \sum_{i=1}^n \mathbf{s}_i^2 + \frac{1}{2} (1 + 2n\lambda) \sum_{i=1}^n \mathbf{u}_i^2. \quad (8.8)$$

Comparing the center-of-mass Hamiltonian to $\frac{1}{2M} \mathbf{P}^2 + \frac{1}{2} M \Omega^2 \mathbf{R}^2$, one sees that $M = n$ and $\Omega = 1$. Therefore the center-of-mass energy is $\Omega = 1$ and the relative energy

$$\omega = \sqrt{1 + 2n\lambda} \quad (8.9)$$

is n -dependent. For attractive interactions, $\lambda > 0$ and $\omega > 1$. For repulsive interactions, $-1/(2n) < \lambda < 0$ and $0 < \omega < 1$, which means that the pairwise repulsion cannot be too strong, otherwise the repulsion will blow up the harmonic confinement. For the ease of knowing the exact ground state energy, we will generally fix ω for all n and set $\lambda = (\omega^2 - 1)/(2n)$.

For the case where each component potential is generalized to

$$V = \frac{1}{2} x^2 \rightarrow \frac{1}{2} \omega^2 x^2 \quad (8.10)$$

it is only necessary to replace

$$\mu_N \rightarrow \mu_N^* = \omega^2 \mu_N, \quad (8.11)$$

in all relevant equations in Sect.III:

$$\begin{aligned} \zeta_N^* &= 1 + \kappa_N \mu_N^* = 1 + \kappa_N \mu_N \omega^2, \\ u^* &= \ln \left(\zeta_1^*(\epsilon) + \sqrt{\zeta_1^{*2}(\epsilon) - 1} \right), \end{aligned} \quad (8.12)$$

$$\gamma^* = \frac{\sqrt{\zeta_1^{*2} - 1}}{\kappa_1}. \quad (8.13)$$

For n fermions, one fills the relative energy spectrum $(n_x + n_y + 1)\omega$ in succession but with its lowest energy state replaced by the center-of-mass energy²⁵. The thermodynamic energy is then given by

$$E_n^T(\tau) = \frac{1}{\sqrt{\zeta_1^2 - 1}} \frac{d\zeta_1}{d\epsilon} E_1(Nu) + \frac{1}{\sqrt{\zeta_1^{*2} - 1}} \frac{d\zeta_1^*}{d\epsilon} (E_n(Nu^*) - E_1(Nu^*)) \quad (8.14)$$

For PA $\zeta_1 = 1 + \epsilon^2/2$, $\zeta_1^* = 1 + \epsilon^2\omega^2/2$, the above reduces to

$$E_n^T(\tau) = \frac{1}{\sqrt{1 + \epsilon^2/4}} E_1(Nu) + \frac{\omega}{\sqrt{1 + \omega^2\epsilon^2/4}} (E_n(Nu^*) - E_1(Nu^*)). \quad (8.15)$$

Note that since $1/\sqrt{1+x} = 1 - x/2 + \dots$, the convergence of the thermodynamic energy is second-order in ϵ and from below the exact energy.

In the continuum limit of $\epsilon \rightarrow 0$ and $\tau \rightarrow \infty$, one has from (5.5), (5.7), (5.9), (B1), $E_1(\tau) \rightarrow 1$, $E_2(\tau) \rightarrow 3$, $E_3(\tau) \rightarrow 5$, $E_4(\tau) \rightarrow 8$, $E_6(\tau) \rightarrow 14$. The above (8.15) then gives

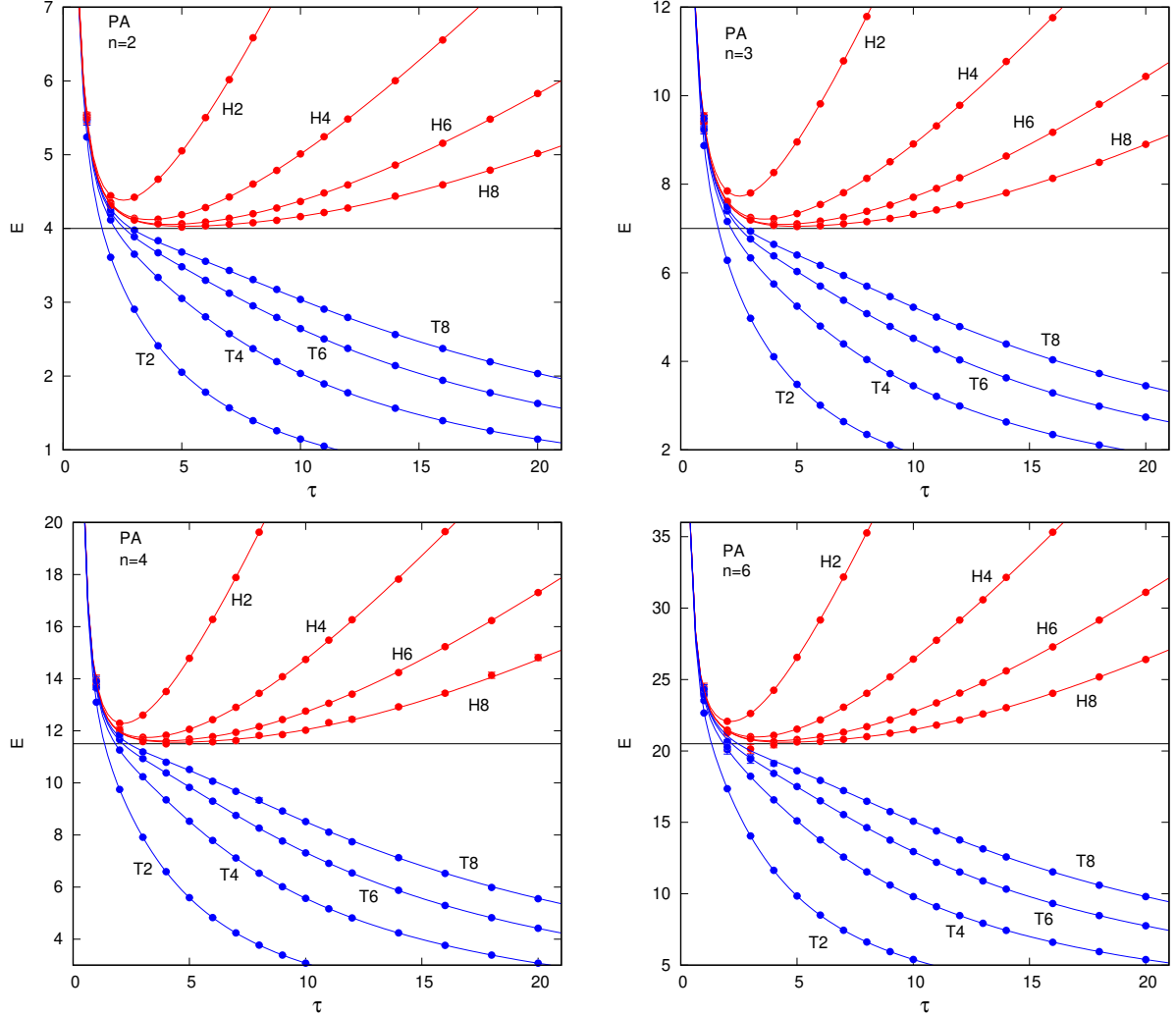


FIG. 6: (color online) The PA propagator's $n = 2, 3, 4$ and 6-fermion N -bead thermodynamic and Hamiltonian energies in a 2D harmonic oscillator with pairwise potential $\lambda(\mathbf{r}_i - \mathbf{r}_j)^2$. The attractive potential strength is set to $\lambda = 5/(8n)$ so that $\omega = 3/2$ for all n . The data points are PIMC calculations and smooth curves are analytical results from (8.15) and (8.18).

the exact ground state fermion energies according to the degeneracy of the 2D harmonic oscillator:

$$E_2^T \rightarrow 1 + 2\omega, \quad E_3^T \rightarrow 1 + 4\omega, \quad E_4^T \rightarrow 1 + 7\omega, \quad E_6^T \rightarrow 1 + 13\omega. \quad (8.16)$$

A careful re-deriving of the Hamiltonian energy as in Ref.15 with $\omega \neq 1$ gives

$$E_n^H(\tau) = \frac{1}{2}(\gamma + \frac{1}{\gamma})E_1(Nu) + \frac{\omega}{2}(\frac{\gamma^*}{\omega} + \frac{\omega}{\gamma^*})(E_n(Nu^*) - E_1(Nu^*)). \quad (8.17)$$

For PA, one has explicitly

$$\begin{aligned} E_n^H(\tau) &= \frac{1}{2} \left(\sqrt{1 + \epsilon^2/4} + \frac{1}{\sqrt{1 + \epsilon^2/4}} \right) E_1(Nu) \\ &+ \frac{\omega}{2} \left(\sqrt{1 + \epsilon^2\omega^2/4} + \frac{1}{\sqrt{1 + \epsilon^2\omega^2/4}} \right) (E_n(Nu^*) - E_1(Nu^*)). \end{aligned} \quad (8.18)$$

Since $(1 + x)^{1/2} + (1 + x)^{-1/2} = 1 + x^2/16 + \dots$, the convergence is now fourth-order in ϵ and from above the exact energy.

The energy convergences of these four n cases are shown in Fig.6, with $\lambda = 5/(8n)$ so that $\omega = 3/2$ for all n values. The exact ground state energies according to (8.16), 4, 7,

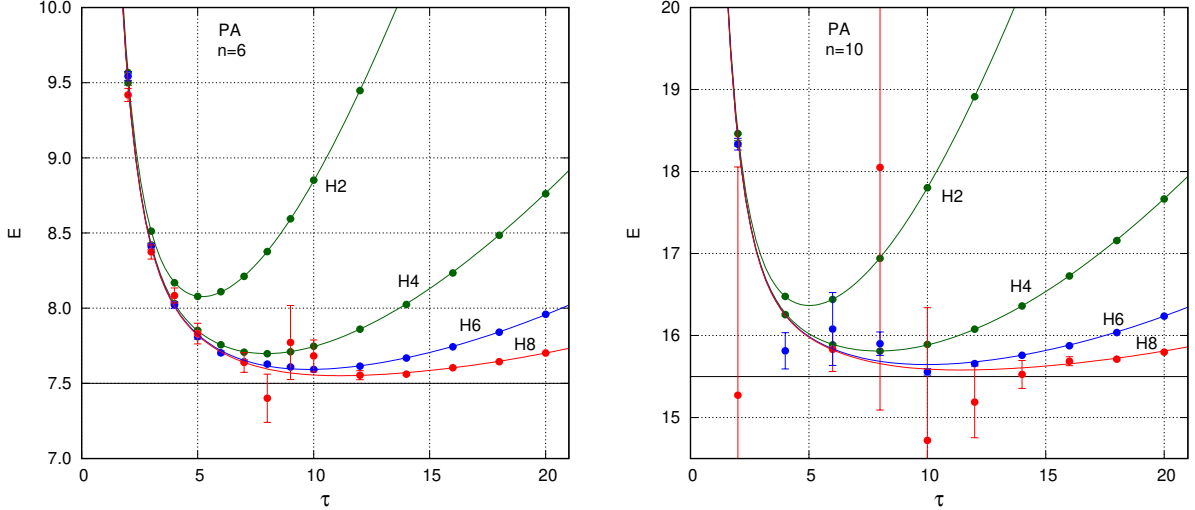


FIG. 7: (color online) The $n = 6$ and 10-fermion N -bead PA Hamiltonian energies in a 2D harmonic oscillator with repulsive pairwise potential $\lambda(\mathbf{r}_i - \mathbf{r}_j)^2$. The repulsive potential strength is set to $\lambda = -3/(8n)$ so that $\omega = 1/2$ for all n . The data points are PIMC calculations and smooth curves are analytical results given by (8.18).

11.5 and 20.5, are shown as horizontal black lines in Fig.6. Again the PIMC results are in perfect agreement with analytical thermodynamic and Hamiltonian energies given by (8.15) and (8.18) respectively. As shown below, the sign problem in these cases are not very severe.

For our main interest in large quantum dots with repulsive pairwise forces, we set $\lambda = -3/(8n)$ so that $\omega = 1/2$ for all n values. The PA Hamiltonian energy for $n = 6$ and $n = 10$ are shown in Fig.7. In contrast to the attractive case, for $n = 6$, H8 is affected by the sign problem with large error bars at $\tau < 10$ but has no problem of reproducing the analytical result at $\tau > 10$. For $n = 10$, H6 and H8 have sign problems below $\tau < 10$ and $\tau < 15$ respectively but none above those values.

These observations can now be understood by examining PA's average sign $s = \langle sgn \rangle$ as a function of interaction strength in Fig.8. One immediately notes that: 1) Attraction ($\lambda > 0$) reduces the overall sign problem as compared to the non-interacting $\lambda = 0$ case, except where $\tau < 2$. This explains the absence of sign problems in Fig.6. 2) Repulsion ($\lambda < 0$) reduces the sign problem at small τ but broadens the sign minimum at large τ . 3) The sign minimum with interaction is never lower than that of the non-interacting case, *i.e.*, pairwise interactions do not worsen the sign problem, only shift the sign minimum to a different τ location.

This suggests that for strong repulsion, one should start at small τ and equilibrate toward the ground state at large τ , as done in Ref.9. For weak to moderate repulsion, it would best

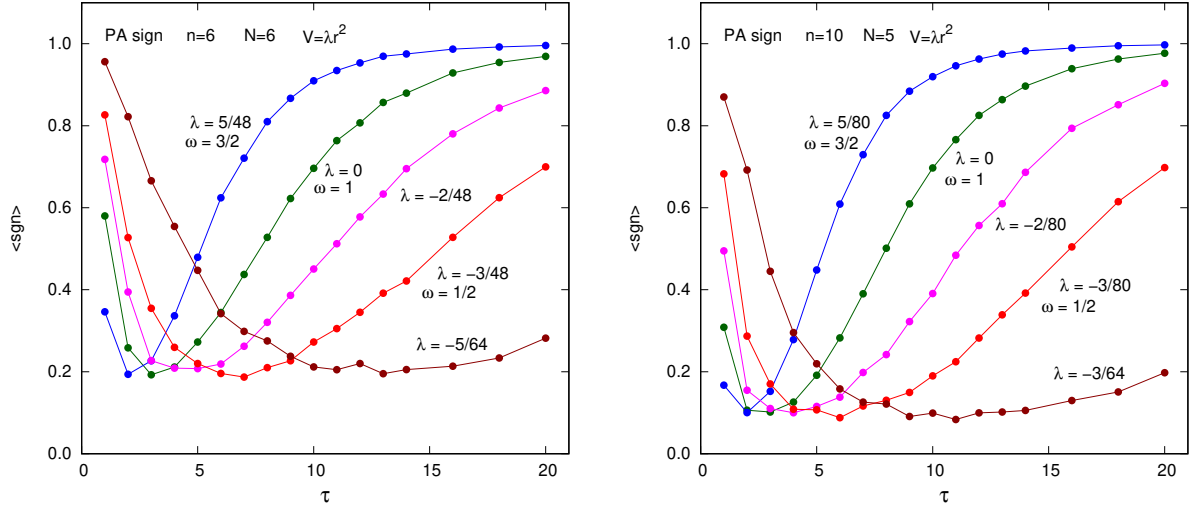


FIG. 8: (color online) The change in the average sign as a function of the strength of the pairwise harmonic interactions for six and ten fermions in a 2D harmonic oscillator.

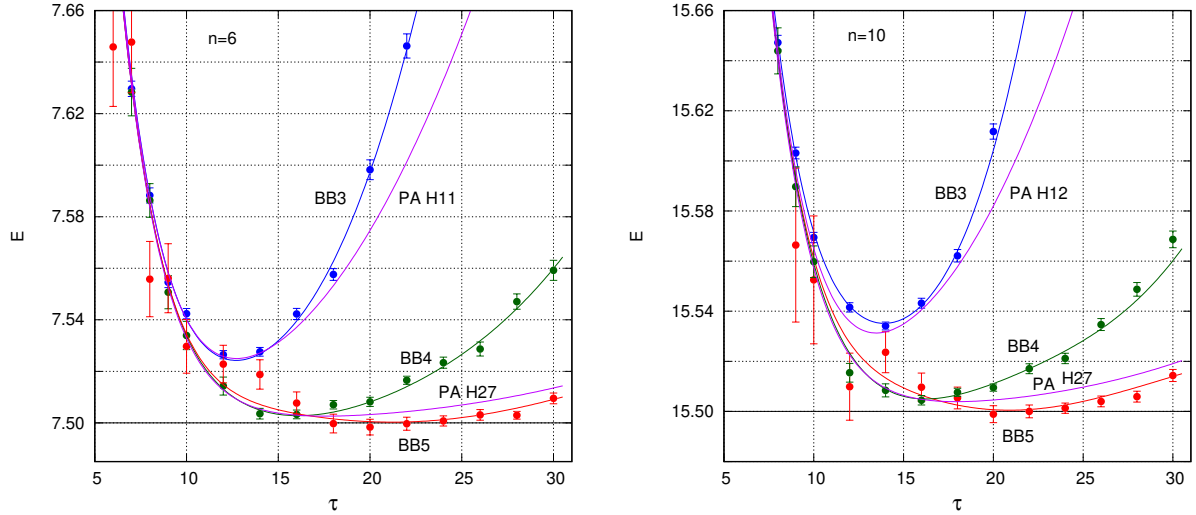


FIG. 9: (color online) Hamiltonian energies for the same $n = 6$ and 10-fermion system as in Fig.7, but solved by three fourth-order propagators as described in Appendix C. The smooth curves are obtained by evaluating (8.17) numerically without knowing its analytical form.

to search for the energy minimum at large τ , where the sign problem is less severe for closed-shell states. However, for PA this strategy can only work at large N , such as H6 and H8 for a small number of fermions in Fig.7. For large n , one must keep N small to control the sign problem.

With repulsive interactions, BB3 can no longer reproduce the exact ground state energy as in the non-interacting case. However, the energy can be greatly improved with BB4 and nearly exactly reproduced by BB5. For up to five beads, the sign problem for $n = 10$ is still manageable with a sign minimum of ≈ 0.1 , similar to the PA case in the right panel of Fig.8. Moreover, as shown in Fig.9, BB3 is comparable to PA H11 for $n = 6$ and comparable to PA H12 for $n = 10$. BB4 is comparable to PA H27 for both cases. These two algorithms are therefore nearly four and seven times as efficient as PA. BB5 is nearly exact, with energy minima of 7.498(3) for $n = 6$ at $\tau = 20$ and 15.499(3) for $n = 10$ also at $\tau = 20$.

For the Coulomb repulsion, the average sign behaves even better. As shown in Fig.10 any Coulomb repulsion lifts the sign minimum above that of the non-interacting case. However, as in the harmonic interaction case, strong repulsion greatly reduces the sign problem at small τ , but suppresses the sign average at large τ , thereby nullifying the closed-shell advantage.

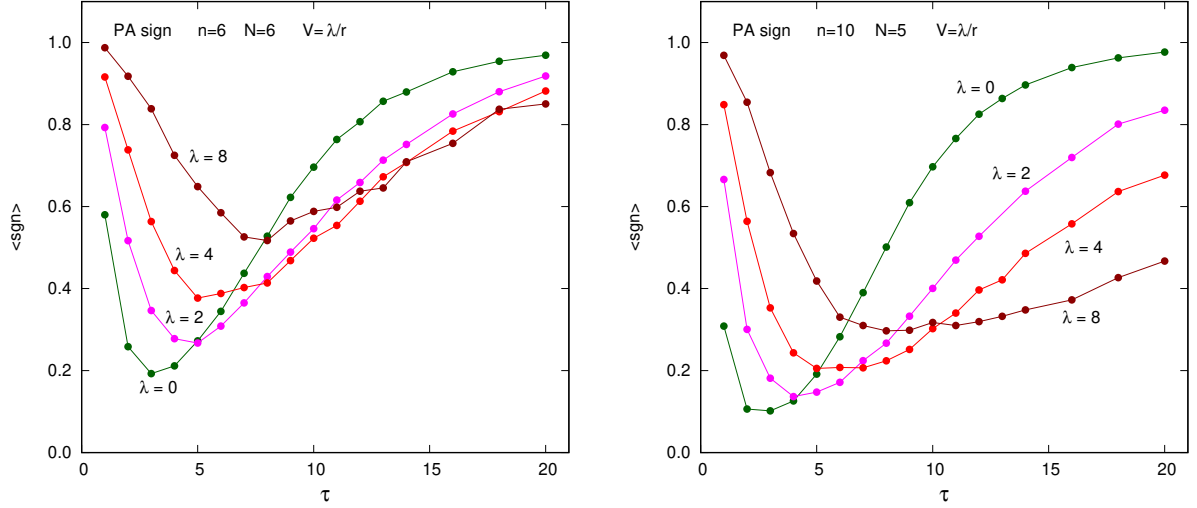


FIG. 10: (color online) The change in the average sign as a function of the strength of the pairwise Coulomb repulsion for six and ten fermions in a 2D harmonic oscillator.

IX. SPIN-BALANCED QUANTUM DOTS

In previous sections, we have studied spin-polarized (or spinless) fermions using a single determinant free propagator. Consider now spin-balanced, unpolarized quantum dots with $n_\uparrow = n_\downarrow = n/2$, where the anti-symmetric free propagator used,

$$\begin{aligned}
 G_0(\mathbf{x}', \mathbf{x}, \epsilon) &= \langle \mathbf{x}' | e^{-\epsilon \hat{T}} | \mathbf{x} \rangle \\
 &= \frac{1}{n_\uparrow!} \det \left(\frac{1}{(2\pi\epsilon)^{D/2}} \exp \left[-\frac{1}{2\epsilon} (\mathbf{r}'_{\uparrow i} - \mathbf{r}'_{\uparrow j})^2 \right] \right) \\
 &\quad \times \frac{1}{n_\downarrow!} \det \left(\frac{1}{(2\pi\epsilon)^{D/2}} \exp \left[-\frac{1}{2\epsilon} (\mathbf{r}'_{\downarrow i} - \mathbf{r}'_{\downarrow j})^2 \right] \right), \tag{9.1}
 \end{aligned}$$

is a product of two determinants. The analytical (or numerical) Hamiltonian energy can be computed by modifying (8.17) to

$$E_n^H(\tau) = \frac{1}{2} \left(\gamma + \frac{1}{\gamma} \right) E_1(Nu) + \frac{\omega}{2} \left(\frac{\gamma^*}{\omega} + \frac{\omega}{\gamma^*} \right) \left(2E_{n/2}(Nu^*) - E_1(Nu^*) \right). \tag{9.2}$$

Since we have the analytical energies $E_3(w)$, $E_6(w)$ and $E_{10}(w)$, we can compute from above, the numerical energies for spin-balanced systems of $n = 6, 12$, and 20 . For $n = 30$, one can again compute $E_{15}(\tau)$ stochastically by using the exact but non-interacting propagator. For repulsive forces such that $\omega = 1/2$ is the same for all n , we compare PIMC data in Fig.11 with their analytical predictions. The spin-balanced case is generally more difficult than the spin-polarized case. This is because even if the two spin-polarized subsystems can be solved

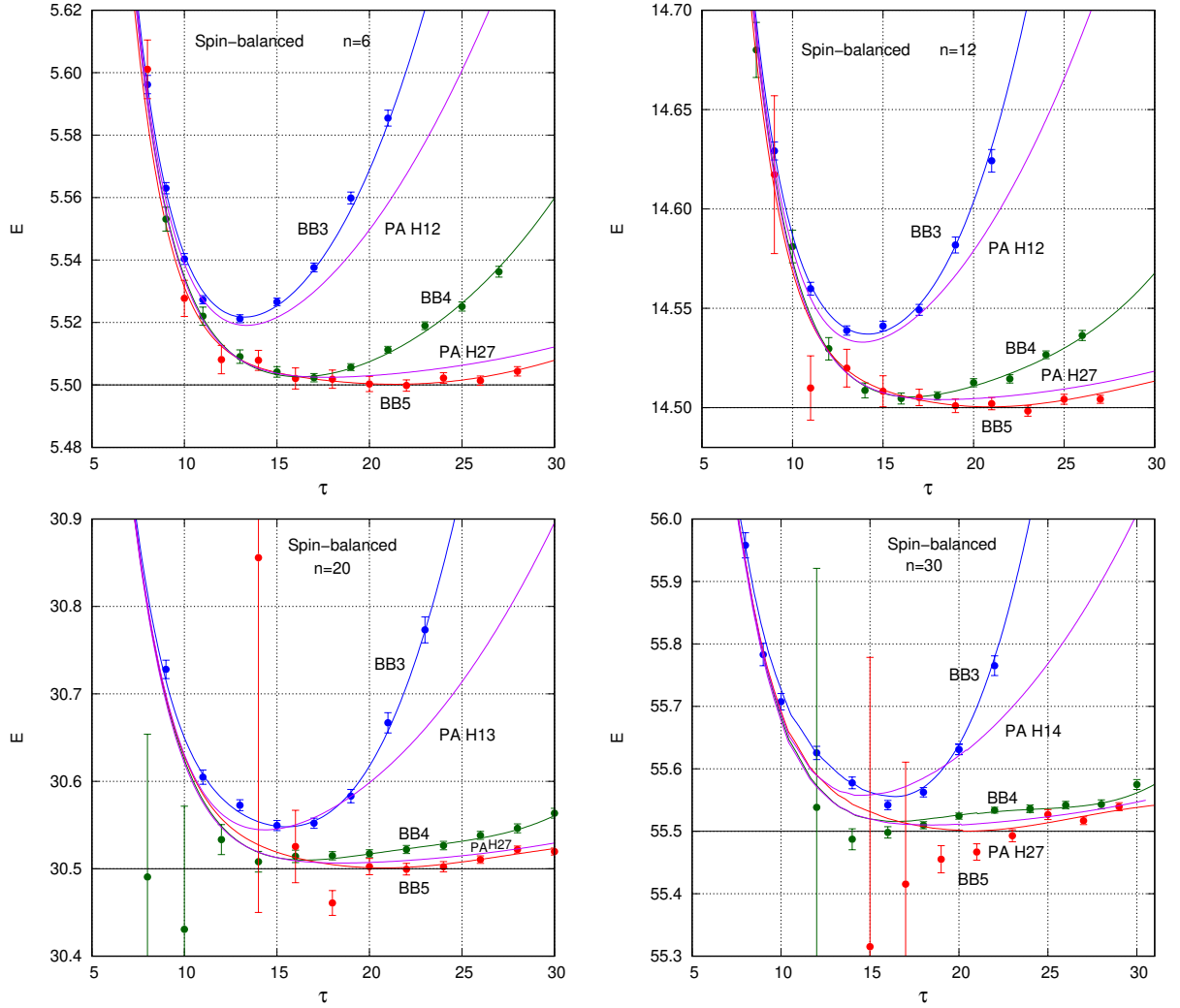


FIG. 11: (color online) Spin-balanced $n = 6, 12, 20, 30$ Hamiltonian energies with pairwise repulsive harmonic potential $\lambda(\mathbf{r}_i - \mathbf{r}_j)^2$ and with λ adjusted so that $\omega = 1/2$ for all n . The data points are PIMC calculations and smooth curves are analytical results given by (9.2). See text for details.

exactly, one still has to account for pairwise interactions between the two subsystems. For harmonic interactions, as seen in Fig.11, the optimized fourth-order algorithms are equally effective in solving spin-balanced cases. However, for $n = 20$, the sign problem for BB5 is very severe below $\tau < 20$, where some data points with very large error bars are outside of the plotting range. For $n = 30$, the sign problem is too severe for BB5, but BB4 can still give excellent estimate of the ground state energy.

For the Coulomb interaction, spin-polarized quantum dots have been studied extensively in Ref.9. For spin-balanced quantum dots, most published works use an alternative

parametrization of the Schrödinger equation

$$(-\frac{1}{2} \sum_{i=1}^n \nabla_i^2 + \frac{1}{2} \sum_{i=1}^n \omega^2 \mathbf{r}_i^2 + \sum_{j>i} \frac{1}{|\mathbf{r}_i - \mathbf{r}_j|})\psi = E_\omega \psi, \quad (9.3)$$

which is related to the interaction form $\lambda/|\mathbf{r}_i - \mathbf{r}_j|$ used here via

$$\lambda = \sqrt{\frac{1}{\omega}} \quad \text{and} \quad E_\omega = E/\lambda^2. \quad (9.4)$$

For the ease of comparing with published works, we will use ω instead of λ as the coupling strength and just denote E_ω as E below. (The ω here has nothing to do with the same symbol used in Eq.(8.9). This should not cause confusion because we will only consider the Coulomb interaction from this point forward.)

The energy results for $n = 6$ are shown in Fig.12. The top-left panel is for $\omega = 0.28$, the coupling closest to the experimental situation. Indicated by horizontal lines are the ground state energies obtained by the method of Hartree-Fock (HF), Couple-Cluster with Single and Double excitation (CCSD), Diffusion Monte Carlo (DMC) by Lohne *et al.*²⁷, the Restricted-path Path Integral Monte Carlo (RPIMC) by Kylänpää and Esa Räsänen²⁸, and the Restricted Boltzmann Machine (RBM) and RBM plus Padè-Jastrow (RBM+PJ) neural network results by Nordhagen *et al.*¹⁶.

The first surprise is that since both RBM and HF are uncorrelated wave functions, it is not clear how RBM can have energy lower than the optimized single-particle wave functions of HF. Second, the HF energy can be bested by PA's H4 and both by H5. The BB3, BB4, BB5 results are, as expected, dramatically lower than those of PA. However, BB5's minimum 7.736(5) at $\tau = 8$, remains 1.8% above the *extrapolated* ground state energy 7.5927(2) of RPIMC and 1.5% above 7.6203(2) of RBM+PJ.

The situation gets worse as one weakens the coupling to $\omega = 0.5$ in the lower-left panel. Here, HF is lower than RBM and H5. BB5's energy of 12.08(1) at $\tau = 8$ is 2.7% above RPIMC's 11.7659(4) and 2.3% above RBM-PJ's 11.80494(7). Weakens the coupling to $\omega = 1.0$ in the lower-right panel shows that HF is below BB5 and BB5's minimum energy of 20.88(2) at $\tau = 7$ is 3.5% above RBM-PJ's 20.1773(1). On the other hand, if one strengthens the coupling to $\omega = 0.1$ (only done in Ref.16), as shown in the upper-right panel, then even H3 is comparable to RBM and BB5's minimum energy of 3.585(4) at $\tau = 8$ is only 0.42% above RBM+PJ's 3.5700(2).

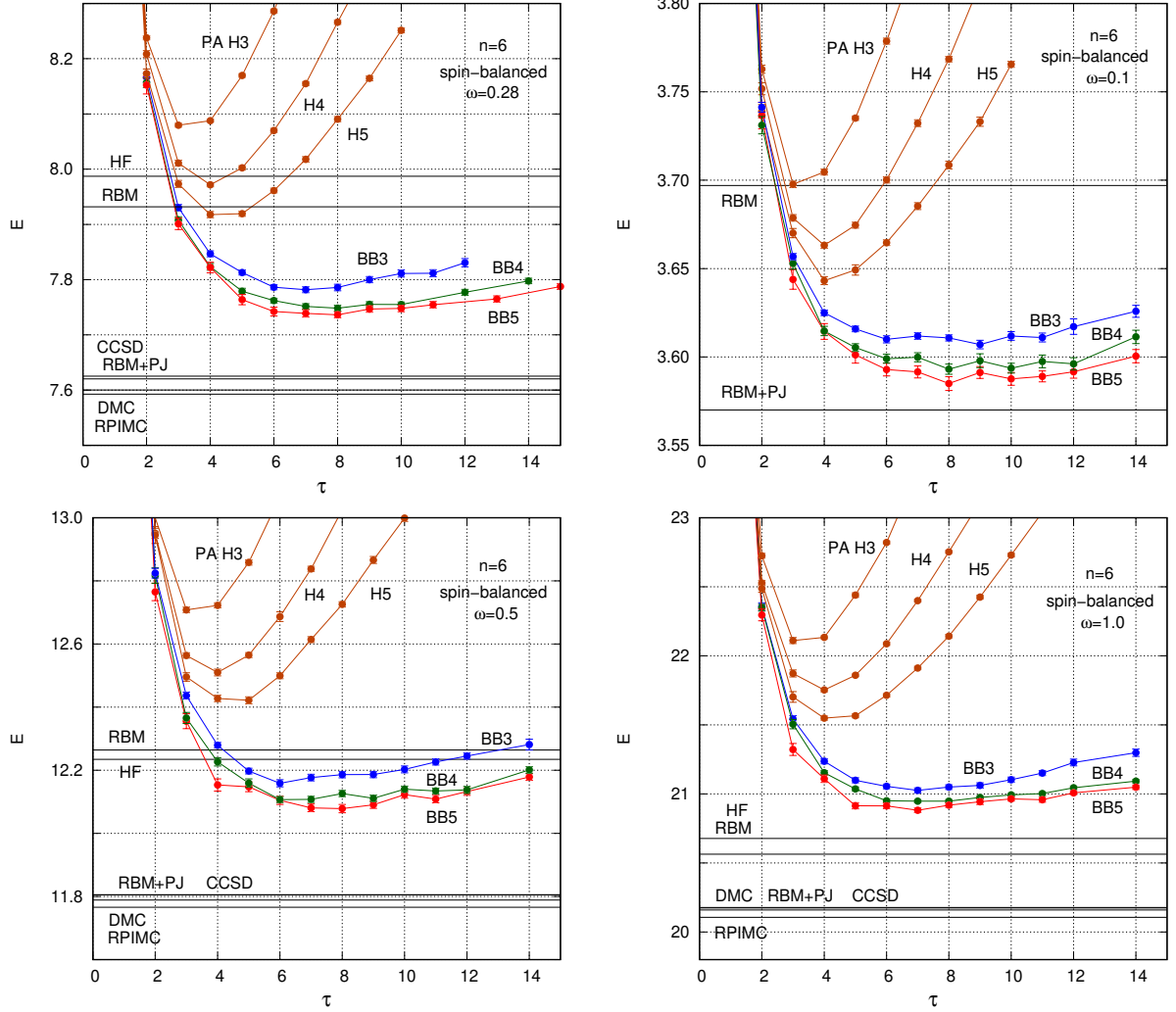


FIG. 12: (color online) The energies of $n = 6$ spin-balanced quantum dots at various values of ω as compared with many published results. See text for details.

This systematic effect is not due to the sign problem, which is manageable for $n = 6$ and N at most 5. This is related to the challenge that faces PIMC in dealing with the singular Coulomb potential, where the exact wave function has cusps. In DMC and RBM+PJ, the cusp condition is built into the trial function. For PIMC, the cusp condition can only be approximated at large N , but this then runs into the sign problem. The present work, which seeks to circumvent the sign problem by restricting $N < 5$, the cusp condition can only be avoided at large couplings, where the strong Coulomb repulsion would keep the particles far apart, away from the cusp of the wave function. This explains the success of Ref.9, which unwittingly, but fortunately, used $\lambda = 8$.

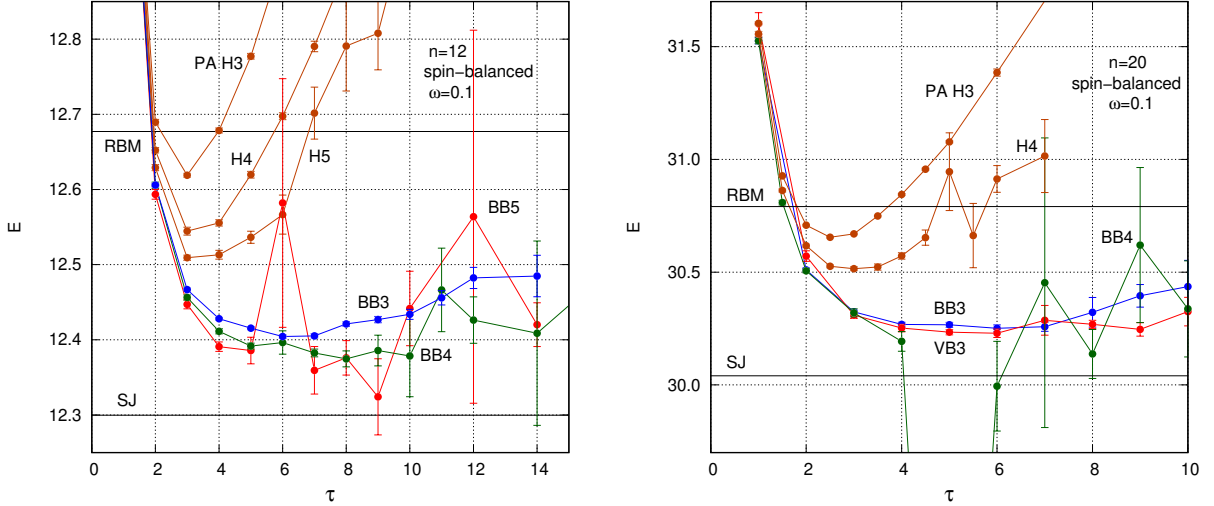


FIG. 13: (color online) Energies of larger $n = 12$ and $n = 20$ unpolarized quantum dots, where the sign problem begins to force out fourth-order propagators. Algorithm VB3 is described in Sect.X.

For $n = 12$ and 20 at $\omega = 0.1$, similar results are shown in Fig.13. For these larger quantum dots, Ref.16's Slater-Jastrow (SJ) based neural network has lower energies. One sees that for $n = 12$ BB5 is barely calculable with large sign errors and cannot be used for $n = 20$. Nevertheless its minimum energy of $12.32(5)$ for $n = 12$ at $\tau = 9$ is only 0.1% above Ref.16's SJ energy of $12.29962(9)$. For $n = 20$, BB4 is barely doable and its energy of $30.19(4)$ at $\tau = 4$ is 0.5% above Ref.16's SJ energy of $30.0403(2)$. For $n = 30$ and larger, not even BB3 is stable. This is consistent with previous energy results on spin-polarized⁹ quantum dots.

X. LARGE QUANTUM DOTS

From Fig.13 one sees that the sign problems for BB5 and BB4 are more severe than their PA counter parts H5 and H4. Evidently, the gradient potential ($\approx 1/r_{ij}^4$) for the pairwise Coulomb interaction, especially at large n , has exacerbated the sign problem. At small N , PA's sign problem seemed more manageable, but its energy is not low enough.

The success of fourth-order propagators is also due to the fact that they have parameters that can be optimized to lower the energy. Surprisingly, such parameters also exist for the PA algorithm. The PA 2-bead propagator given by

$$\hat{G}_2(\epsilon) = e^{-\frac{1}{2}\epsilon\hat{V}} e^{-\epsilon\hat{T}} e^{-\epsilon\hat{V}} e^{-\epsilon\hat{T}} e^{-\frac{1}{2}\epsilon\hat{V}}, \quad (10.1)$$

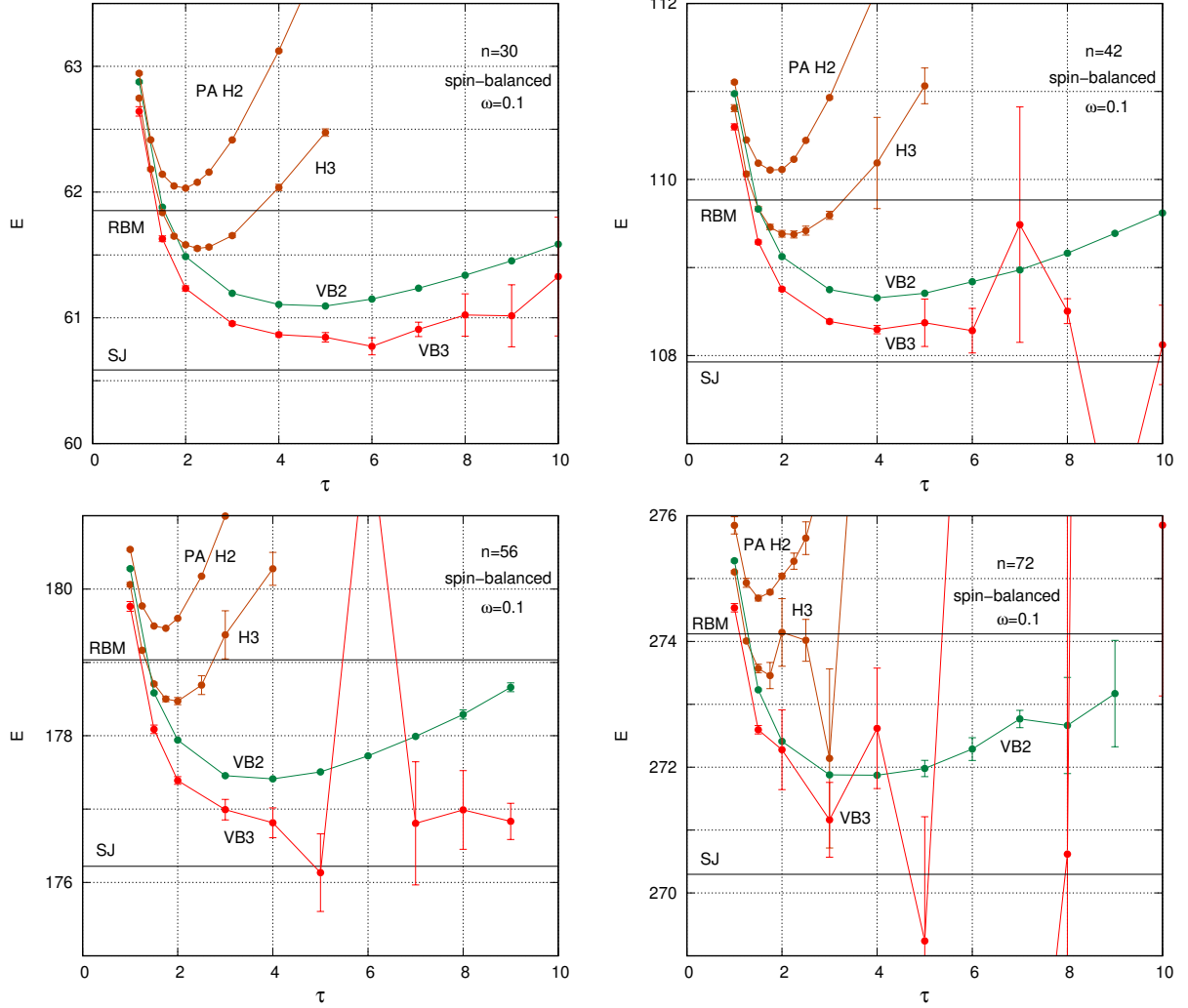


FIG. 14: (color online) Large quantum dot calculations using Variable-Bead propagators VB2 and VB3. See text for details.

has a hidden parameter v_1 ,

$$\hat{G}_2(\epsilon) = e^{-\frac{1}{2}v_1\epsilon\hat{V}}e^{-\epsilon\hat{T}}e^{-(2-v_1)\epsilon\hat{V}}e^{-\epsilon\hat{T}}e^{-\frac{1}{2}v_1\epsilon\hat{V}}. \quad (10.2)$$

As long as the propagator remains left-right symmetric, it is second-order. The case of $v_1 = 1$ reproduces the original PA of (10.1) and $v_1 = 2$ gives PA at step size 2ϵ . Clearly then, PA can only be improved for $v_1 < 1$. In Fig.14, we show its energy for $n = 30, 42, 56$ and 72 quantum dots at $v_1 = 0.25$. Its energy is dramatically lower than the unvarnished PA H2. Its energy minima, recorded in Table I, are midway between that of RBM and SJ for all n . We shall refer to this as the Variable-Bead, VB2 propagator. VB2, like PA H2, has no sign problem.

TABLE I: Comparing this work's VB2 and VB3 spin-balanced quantum dot ground state energies at coupling $\omega = 0.1$ with those of RBM and SJ neural networks¹⁶.

| n | RBM ¹⁶ | VB2 | VB3 | SJ ¹⁶ |
|-----|-------------------|-----------|-----------|------------------|
| 30 | 61.853(2) | 61.094(5) | 60.77(7) | 60.585(1) |
| 42 | 109.767(7) | 108.65(1) | 108.29(5) | 107.928(2) |
| 56 | 179.035(8) | 177.41(1) | 176.8(2) | 176.221(1) |
| 72 | 274.12(1) | 271.87(1) | 271.2(6) | 270.296(3) |
| 90 | 399.84(1) | 396.69(6) | ... | 394.621(4) |
| 110 | ... | 556.5(6) | ... | ... |

For 3-bead, one can choose the two free parameters v_1 and t_1 more concisely as follow:

$$\hat{G}_3(\epsilon) = e^{-\frac{1}{2}(3-2v_1)\epsilon\hat{V}} e^{-t_1\epsilon\hat{T}} e^{-v_1\epsilon\hat{V}} e^{-(3-2t_1)\epsilon\hat{T}} e^{-v_1\epsilon\hat{V}} e^{-t_1\epsilon\hat{T}} e^{-\frac{1}{2}(3-2v_1)\epsilon\hat{V}}. \quad (10.3)$$

One recovers PA H3 at $v_1 = 1$, $t_1 = 1$, and $v_1 = 0$ collapses the propagator to that of PA at step size 3ϵ . For $t_1 = 0.5$ and $v_1 = 1.4$, the minimum energy of this VB3 propagator for $n = 30, 42, 56, 72$ at $\tau = 6, 4, 4, 3$, is shown in Fig.14 and recorded in Table I. All are only only 0.3% above Ref.16's SJ energy. By contrast, VB2's energies at $\tau = 5, 4, 4$ and 4 are 0.8%, 0.7%, 0.7% and 0.6% above Ref.16's SJ energy respectively.

Our error bars are much larger because each calculation was done sampling at most 2×10^7 particle-configurations on desktop computers. From Fig.13, for $n = 20$, VB3 is comparable to BB3, despite being only a second-order algorithm.

For $n = 72$, VB3 has huge sign errors. For $n = 90$, VB3 is no longer stable and only VB2 can be applied in Fig.1. Nevertheless, VB2's energy is only 0.5% higher than Ref.16's SJ energy. For $n = 110$, also shown in Fig.1, there is no published energy for such a large quantum dot. If VB2's energy remains about 0.5% above the ground state energy, then the ground state energy can be inferred to be approximately 553.7, plotted as a dash line in Fig.1.

The energy results in Fig.1 took weeks to produce on multiple desktop computers. It is at the limit of what personal computers can do.

XI. CONCLUSIONS AND FUTURE DIRECTIONS

In this work we have formulated a completely solvable PIMC model of harmonic fermions with and without pairwise harmonic interactions where the Hamiltonian energy and the sign problem can be studied in details as functions of bead and fermion numbers. We showed that strong pairwise repulsion reduces/enhances the sign problem at short/long imaginary time. We explained the connection between the absence of the sign problem in one dimension and in closed-shell states. We showed that fourth-order short-time propagators are effective in determining ground state energies of less than 30 fermions with pairwise harmonic interactions or for sufficiently repulsive Coulomb forces. For spin-balance, unpolarized quantum dots with 30 or more electrons, the pairwise gradient potential is too singular for fourth-order methods to be used. However, this work found a new class of Variable-Bead algorithms which yielded ground state energies that are only 0.5% or less above modern neural network results for up to 90 electrons. This was completely unexpected. The efficiency of this class of algorithms should be further tested on other quantum systems.

Path integral Monte Carlo is the granddaddy of modern neural network in that it is the only traditional quantum Monte Carlo method with build-in “hidden-layers”. When PA is used, these layers are completely known and fixed. The Variable-Bead propagators have hidden-layer parameters that can be fine-tuned, making them similar to neural networks. However, these parameters do not alter the fundamental Gaussian nature of PIMC, and therefore cannot overcome the fundamental challenge of dealing singular potentials. Propagators such as (10.2) and (10.3) are actually ways of approximating the *square* of the wave function. Perhaps one can learn from neural networks and replaces the free propagator’s Gaussian determinant by a more general type of determinant, similar to the way Ref.29’s neural network is parametrizing the exact wave function.

On the other hand, the VB2 and VB3 algorithms used here are much, much simpler than any fermion neural network^{16,29}, suggesting that neural networks may also benefit from knowing the structure of PIMC in their search for the ground state wave function.

AUTHOR DECLARATIONS

Conflict of Interest

The authors have no conflicts to disclose.

Author Contributions

Siu A. Chin: Conceptualization (lead); Formal analysis (lead); Visualization (lead); Writing—original draft (lead).

DATA AVAILABILITY

The data that supports the findings of this study are available within the article and by inquiry to the author.

Appendix A: Needed integrals

The fundamental integral needed is

$$z_n = \frac{1}{(2\pi\kappa_N)^{nD/2}} \int d\mathbf{r}_1 d\mathbf{r}_2 \cdots d\mathbf{r}_n e^{-\mu_N(\mathbf{r}_1^2 + \mathbf{r}_2^2 + \cdots + \mathbf{r}_n^2)} e^{-(\mathbf{r}_{12}^2 + \mathbf{r}_{23}^2 + \cdots + \mathbf{r}_{n1}^2)/2\kappa_N}. \quad (\text{A1})$$

This is the trace of the propagator

$$G_n(\mathbf{r}_1, \mathbf{r}_{n+1}) = G_1(\mathbf{r}_1, \mathbf{r}_2) G_1(\mathbf{r}_2, \mathbf{r}_3) \cdots G_1(\mathbf{r}_n, \mathbf{r}_{n+1}) \quad (\text{A2})$$

where

$$G_1(\mathbf{r}_i, \mathbf{r}_j) = \frac{1}{(2\pi\kappa_N)^{D/2}} e^{-\mu_N \mathbf{r}_i^2/2} e^{-\mathbf{r}_{ij}^2/2\kappa_N} e^{-\mu_N \mathbf{r}_j^2/2}. \quad (\text{A3})$$

This $G_1(\mathbf{r}_i, \mathbf{r}_j)$ can be regarded as a short-time propagator with coefficients $\tilde{\mu}_1$ and $\tilde{\kappa}_1$ given as

$$\tilde{\mu}_1 = \mu_N \quad \text{and} \quad \tilde{\kappa}_1 = \kappa_N. \quad (\text{A4})$$

Therefore, by contracting the fermion number n ,

$$G_n(\mathbf{r}_1, \mathbf{r}_{n+1}) = \frac{1}{(2\pi\tilde{\kappa}_n)^{D/2}} e^{-\tilde{\mu}_n \mathbf{r}_1^2/2} e^{-(\mathbf{r}_1 - \mathbf{r}_{n+1})^2/2\tilde{\kappa}_n} e^{-\tilde{\mu}_n \mathbf{r}_{n+1}^2/2}, \quad (\text{A5})$$

one has the trace

$$\begin{aligned} z_n &= \frac{1}{(2\pi\tilde{\kappa}_n)^{D/2}} \int d\mathbf{r}_1 e^{-\tilde{\mu}_n \mathbf{r}_1^2} = \frac{1}{(2\pi\tilde{\kappa}_n)^{D/2}} \left(\frac{\pi}{\tilde{\mu}_n} \right)^{D/2} \\ &= \frac{1}{[2(\tilde{\zeta}_n - 1)]^{D/2}} = \frac{1}{[2 \sinh(n\tilde{u}/2)]^D}. \end{aligned} \quad (\text{A6})$$

From the fundamental definition of \tilde{u} ,

$$\cosh(\tilde{u}) = \tilde{\zeta}_1 = \zeta_N = \cosh(Nu) \quad \rightarrow \quad \tilde{u} = Nu, \quad (\text{A7})$$

one then easily arrives at

$$z_n = \frac{1}{[2 \sinh(nNu/2)]^D}. \quad (\text{A8})$$

Appendix B: Discrete n-fermion energies

The discrete n -fermion energies in 2D, for $n = 4, 5, 6, 10$, are given by

$$E_n(w) = \frac{\mathcal{N}_n(w)}{\mathcal{D}_n(w)} \quad (\text{B1})$$

where

$$\begin{aligned}
\mathcal{N}_4(w) &= 2(99 + 196 \cosh(w) + 140 \cosh(2w) + 96 \cosh(3w) + 33 \cosh(4w) + 12 \cosh(5w)) \\
\mathcal{D}_4(w) &= 14 \sinh(w) + 18 \sinh(2w) + 17 \sinh(3w) + 7 \sinh(4w) + 3 \sinh(5w) \\
\mathcal{N}_5(w) &= 4711 + 8989 \cosh(w) + 7731 \cosh(2w) + 5999 \cosh(3w) + 4113 \cosh(4w) \\
&\quad + 2479 \cosh(5w) + 1245 \cosh(6w) + 532 \cosh(7w) + 168 \cosh(8w) + 33 \cosh(9w) \\
\mathcal{D}_5(w) &= 117 \sinh(w) + 197 \sinh(2w) + 223 \sinh(3w) + 197 \sinh(4w) + 143 \sinh(5w) \\
&\quad + 83 \sinh(6w) + 40 \sinh(7w) + 14 \sinh(8w) + 3 \sinh(9w) \\
\mathcal{N}_6(w) &= 2(13407 + 25721 \cosh(w) + 23643 \cosh(2w) + 20003 \cosh(3w) + 16124 \cosh(4w) \\
&\quad + 11811 \cosh(5w) + 8284 \cosh(6w) + 5100 \cosh(7w) + 2994 \cosh(8w) + 1495 \cosh(9w) \\
&\quad + 697 \cosh(10w) + 231 \cosh(11w) + 83 \cosh(12w) + 7 \cosh(13w)) \\
\mathcal{D}_6(w) &= 319 \sinh(w) + 586 \sinh(2w) + 736 \sinh(3w) + 783 \sinh(4w) + 707 \sinh(5w) \\
&\quad + 588 \sinh(6w) + 415 \sinh(7w) + 275 \sinh(8w) + 152 \sinh(9w) \\
&\quad + 78 \sinh(10w) + 28 \sinh(11w) + 11 \sinh(12w) + \sinh(13w) \\
\mathcal{N}_{10}(w) &= 2(2172390222 + 4314823362 \cosh(w) + 4226750929 \cosh(2w) + 4083387729 \cosh(3w) \\
&\quad + 3890856869 \cosh(4w) + 3655779444 \cosh(5w) + 3387254600 \cosh(6w) \\
&\quad + 3094022640 \cosh(7w) + 2786204840 \cosh(8w) + 2472642591 \cosh(9w) \\
&\quad + 2162513611 \cosh(10w) + 1863006410 \cosh(11w) + 1580890927 \cosh(12w) \\
&\quad + 1320648075 \cosh(13w) + 1085993727 \cosh(14w) + 878480571 \cosh(15w) \\
&\quad + 698947301 \cosh(16w) + 546512238 \cosh(17w) + 419881330 \cosh(18w) \\
&\quad + 316639653 \cosh(19w) + 234330752 \cosh(20w) + 169951624 \cosh(21w) \\
&\quad + 120771356 \cosh(22w) + 83937273 \cosh(23w) + 57045201 \cosh(24w) \\
&\quad + 37816435 \cosh(25w) + 24450854 \cosh(26w) + 15364872 \cosh(27w) \\
&\quad + 9385562 \cosh(28w) + 5543351 \cosh(29w) + 3168210 \cosh(30w) \\
&\quad + 1737590 \cosh(31w) + 916301 \cosh(32w) + 457947 \cosh(33w)
\end{aligned}$$

$$\begin{aligned}
& +218192 \cosh(34w) + 96260 \cosh(35w) + 39986 \cosh(36w) + 14646 \cosh(37w) \\
& +4935 \cosh(38w) + 1274 \cosh(39w) + 295 \cosh(40w) + 15 \cosh(41w)
\end{aligned}$$

$$\begin{aligned}
\mathcal{D}_{10}(w) = & 6269567 \sinh(w) + 12284154 \sinh(2w) + 17803408 \sinh(3w) + 22622674 \sinh(4w) \\
& +26575827 \sinh(5w) + 29556940 \sinh(6w) + 31508496 \sinh(7w) \\
& +32440172 \sinh(8w) + 32402745 \sinh(9w) + 31504002 \sinh(10w) \\
& +29872385 \sinh(11w) + 27671748 \sinh(12w) + 25061386 \sinh(13w) \\
& +22212164 \sinh(14w) + 19268782 \sinh(15w) + 16369539 \sinh(16w) \\
& +13614501 \sinh(17w) + 11088828 \sinh(18w) + 8838635 \sinh(19w) \\
& +6895528 \sinh(20w) + 5259530 \sinh(21w) + 3922450 \sinh(22w) \\
& +2855501 \sinh(23w) + 2029305 \sinh(24w) + 1404510 \sinh(25w) \\
& +946820 \sinh(26w) + 619536 \sinh(27w) + 393644 \sinh(28w) + 241576 \sinh(29w) \\
& +143348 \sinh(30w) + 81552 \sinh(31w) + 44588 \sinh(32w) + 23086 \sinh(33w) \\
& +11394 \sinh(34w) + 5203 \sinh(35w) + 2238 \sinh(36w) + 848 \sinh(37w) \\
& +296 \sinh(38w) + 79 \sinh(39w) + 19 \sinh(40w) + \sinh(41w)
\end{aligned} \tag{B2}$$

In the continuum limit of $u \rightarrow \epsilon$, $w \rightarrow \tau$, these are then the exact n -fermion energy as a function of τ .

Appendix C: Fourth-order algorithms

Positive time-step fourth-order short-time propagators with arbitrary number of T operators, or beads, have been derived in Ref.26. For completeness, we will briefly summarize their operator form as done in Ref.9. Consider a short-time propagator with $(N - 1)$ beads of the form

$$\mathcal{T}_{(N-1)B}^{(4)}(\epsilon) = e^{v_1 \epsilon V} e^{t_2 \epsilon T} e^{v_2 \epsilon V} \cdots e^{t_N \epsilon T} e^{v_N \epsilon V} \tag{C1}$$

with left-right symmetric coefficients $v_1 = v_N$, $t_2 = t_N$, etc.. This operator will be fourth-order if one chooses $\{t_i\} > 0$ satisfying $\sum_{i=1}^N t_i = 1$, and $\{v_i\}$ given by

$$v_1 = v_N = \frac{1}{2} + \lambda_2(1 - t_2), \quad v_i = -\lambda_2(t_i + t_{i+1}), \tag{C2}$$

where $\lambda_2 = -\phi^{-1}/2$, $\phi = 1 - \sum_{i=1}^N t_i^3$, and the gradient coefficient $u_0 = (1/\phi - 1)/24$ with the gradient potential term $u_0 \epsilon^3 [V, [T, V]]$ distributed left-right symmetrically among all the $v_i \epsilon V$ terms in (C1). In order not to complicate the evaluation of Hamiltonian energy, the gradient potential term must *not* be distributed to the v_1 and v_N potential terms.

To illustrate the above equations, consider the case of a 3-bead propagator with $N = 4$. One then must have $t_2 + t_3 + t_4 = 2t_2 + t_3 = 1$ and therefore $t_3 = 1 - 2t_2$, with t_2 a free parameter in the range $0 \leq t_2 \leq 1/2$. One can then compute that $\phi = 6t_2(1 - t_2)^2$ and $u_0 = (1/(6t_2(1 - t_2)^2) - 1)/24$, reproducing the \mathcal{T}_{BDA} propagator in Ref.14 with minor changes in notation. The Hamiltonian energy can then be optimized by varying t_2 to give the Best 3-Bead algorithm BB3. Its effectiveness in solving for the non-interacting fermion energies is shown in Fig.3.

Similarly, one can derive the Best 4-Bead algorithm BB4 with the additional freedom of distributing the gradient term between the central $v_3 V$ and the two adjacent $v_2 V$ potential terms. For a BB5 algorithm, one has free parameters t_2 , t_3 and the freedom to distribute the gradient term to the two inner or the two further out potential terms.

If the universal energy $E_n(w)$ is known, then any algorithm of the form (C1), with given parameter values, can be contracted *numerically* down to κ_1 and μ_1 to determine $\gamma(\epsilon)$ and therefore the Hamiltonian energy via (5.15), (8.17) or (9.2).

Appendix D: Average sign at large τ

To compute the average sign $s = \langle sgn \rangle$ for the two-fermion propagator in the three-bead case, one recalls (7.4). In the large τ limit, one can ignore all radial integration. For a closed loop one has

$$s_3 = \frac{\int_{-\pi}^{\pi} d\phi_1 \int_{-\pi}^{\pi} d\phi_2 \cos(\phi_1) \cos(\phi_2) \cos(\phi_1 + \phi_2)}{\int_{-\pi}^{\pi} d\phi_1 \int_{-\pi}^{\pi} d\phi_2 |\cos(\phi_1) \cos(\phi_2) \cos(\phi_1 + \phi_2)|} = \frac{I}{J} \quad (\text{D1})$$

which by symmetry

$$I = \int_0^{\pi} d\phi_1 \int_0^{\pi} d\phi_2 \cos(\phi_1) \cos(\phi_2) \cos(\phi_1 + \phi_2) = \frac{\pi^2}{4}. \quad (\text{D2})$$

The integrand of I has two negative triangular regions bounded by $\phi_1 = \pi/2$, $\phi_2 = \pi/2$, $\phi_1 + \phi_2 = \pi/2$, and $\phi_1 = \pi/2$, $\phi_2 = \pi/2$, $\phi_1 + \phi_2 = 3\pi/2$. Both integrated to $-(12 - \pi^2)/32$. Hence

$$J = \frac{\pi^2}{4} + \frac{12 - \pi^2}{8} = \frac{12 + \pi^2}{8}, \quad (\text{D3})$$

and

$$s_3 = \frac{2\pi^2}{12 + \pi^2} = 0.902586. \quad (\text{D4})$$

For the general N -bead case,

$$s_N = \frac{\int_{-\pi}^{\pi} d\phi_1 d\phi_2 \cdots d\phi_{N-1} \cos(\phi_1) \cos(\phi_2) \cdots \cos(\phi_{N-1}) \cos(\sum_{k=1}^{N-1} \phi_k)}{\int_{-\pi}^{\pi} d\phi_1 d\phi_2 \cdots d\phi_{N-1} |\cos(\phi_1) \cos(\phi_2) \cdots \cos(\phi_{N-1}) \cos(\sum_{k=1}^{N-1} \phi_k)|}, \quad (\text{D5})$$

the integral can be done numerically, either by quadrature (for small N) or by Monte Carlo (for larger N). One then finds that $s_4 = 0.7426$, $s_5 = 0.5927$, $s_6 = 0.4680$, and $s_8 = 0.2890$.

* Electronic address: `chin@physics.tamu.edu`.

- ¹ S. Jang, S. Jang and G. A. Voth, “Applications of higher order composite factorization schemes in imaginary time path integral simulations”, *J. Chem. Phys.* **115** 7832, (2001).
- ² K. Sakkos, J. Casulleras, and J. Boronat, “High order Chin actions in path integral Monte Carlo”, *J. Chem. Phys.* **130**, 204109 (2009).
- ³ R.E. Zillich, J.M. Mayrhofer, S.A. Chin, “Extrapolated high-order propagators for path integral Monte Carlo simulations”, *J. Chem. Phys.* 132 (4) (2010)
- ⁴ Y. Kamibayashi and S. Miura, “Variational path integral molecular dynamics and hybrid Monte Carlo algorithms using a fourth order propagator with applications to molecular systems ”, *J. Chem. Phys.* **145**, 074114 (2016).
- ⁵ V. Kapil, J. Behler and M. Ceriotti “High order path integrals made easy” *J. Chem. Phys.* **145**, 234103 (2016)
- ⁶ Y. Yan and D. Blume, “Path integral Monte Carlo ground state approach: Formalism, implementation, and applications”, *J. Phys. B: At. Mol. Opt. Phys.* 50, 223001 (2017).
- ⁷ L. P. Lindoy, G. S. Huang, and M. J. T. Jordan, “Path integrals with higher order actions: Application to realistic chemical systems” *J. Chem. Phys.* **148**, 074106 (2018).
- ⁸ C. Wang, L. Zhang, J. Liu, J. Shao, “Generalized Fourth-Order Decompositions of Imaginary Time Path Integral: Implications of the Harmonic Oscillator” *Chinese J. Chem. Phys.* **35**, 516-536 (2022).
- ⁹ S. A. Chin, “High-order path-integral Monte Carlo methods for solving quantum dot problems”, *Phys. Rev. E* **91**, 031301(R) (2015)

¹⁰ T. Dornheim et al, “Permutation blocking path integral Monte Carlo: a highly efficient approach to the simulation of strongly degenerate non-ideal fermions” *New J. Phys.* **17**, 073017 (2015)

¹¹ T. Dornheim, S. Groth and M. Bonitz, “The Uniform Electron Gas at Warm Dense Matter Conditions”, *Physics Reports*, 744, 1-86 (2018).

¹² M. Takahashi and M. Imada, “Monte Carlo calculation of quantum systems” *J. Phys. Soc. Jpn.* **53**, 963 (1984).

¹³ S. A. Chin, “Simple proof that there is no sign problem in path integral Monte Carlo simulations of fermions in one dimension” *Phys. Rev. E* **109**, 065312 (2024).

¹⁴ S. A. Chin “Anatomy of Path Integral Monte Carlo: algebraic derivation of the harmonic oscillator’s universal discrete imaginary-time propagator and its sequential optimization ”, *J. Chem. Phys.* **159**, 134109 (2023); doi: 10.1063/5.0164086

¹⁵ S. A. Chin “Analytical evaluations of the path integral Monte Carlo thermodynamic and Hamiltonian energies for the harmonic oscillator”, *J. Chem. Phys.* **159**, 244104 (2023); doi: 10.1063/5.0181447

¹⁶ E. M. Nordhagen, J. M. Kim, B. Fore, A. Lovato and M Hjorth-Jensen, “Efficient solutions of fermionic systems using artificial neural networks” *Front. Phys.* **11**, 1-14 (2023).

¹⁷ D. M. Ceperley, “Path Integrals in the Theory of Condensed Helium”, *Rev. Mod. Phys.* **67**, 279 (1995).

¹⁸ A. P. Lyubartsev, “Simulation of excited states and the sign problem in the path integral Monte Carlo method” *J. Phys. A: Math. Gen.* **38**, 6659 (2005).

¹⁹ D. I. Ford, “A Note on the Partition Function for Systems of Independent Particles”, *Am. J. Phys.* **39**, 215 (1971).

²⁰ P. Borrmann and G. Franke, “Recursion formulas for quantum statistical partition functions” *J. Chem. Phys.* **98** , 2484 (1993).

²¹ A. Chaudhary, “Newton’s identity in Fermionic Partition Function”, 2023, unpublished.

²² M. Troyer and U.-J. Wiese, “Computational complexity and fundamental limitations to fermionic quantum Monte Carlo simulations”, *Phys. Rev. Lett.* **94**, 170201 (2005).

²³ T. Dornheim, “Fermion sign problem in path integral Monte Carlo simulations: Quantum dots, ultracold atoms, and warm dense matter”, *Phys. Rev. E* **100**, 023307 (2019)

²⁴ F. Brosens, J. T. Devreese and L. F. Lemmens, “Thermodynamics of coupled identical oscillators within the path-integral formalism” *Phys. Rev. E* **55**, 227 (1997).

²⁵ F. Brosens, J. T. Devreese and L. F. Lemmens, “Confined harmonically interacting spin-polarized fermions”, Phys. Rev. E **57**, 3871 (1998).

²⁶ S. A. Chin, “A fundamental theorem on the structure of symplectic integrators” Phys. Lett. A **354**, 373–376 (2006).

²⁷ M. Pedersen Lohne, G. Hagen, M. Hjorth-Jensen, S. Kvaal and F. Pederiva, “Ab initio computation of the energies of circular quantum dots” Phys. Rev. B **84**, 115302 (2011).

²⁸ Ilkka Kylänpää and Esa Räsänen, “Path integral Monte Carlo benchmarks for two-dimensional quantum dots” Phys. Rev. B **96**, 205445 (2017)

²⁹ D. Pfau, J. S. Spencer, A.G.D.G Matthews, W. M. C. Foulkes, “Ab initio solution of the many-electron Schrödinger equation with deep neural networks” Phys Rev Res **2**, 033429 (2020).